Central role for PICALM in amyloid–ß blood–brain barrier transcytosis and clearance

HHS Public Access

Author manuscript

Nat Neurosci. Author manuscript; available in PMC 2016 January 01.

Published in final edited form as:

Nat Neurosci. 2015 July ; 18(7): 978–987. doi:10.1038/nn.4025.

Central role for PICALM in amyloid–β blood–brain barrier transcytosis and clearance

Zhen Zhao[1,10], **Abhay P. Sagare**[1,10], **Qingyi Ma**[1,10], **Matthew R. Halliday**[1], **Pan Kong**[1], **Kassandra Kisler**[1], **Ethan A. Winkler**[1,2], **Anita Ramanathan**[1], **Takahisa Kanekiyo**[3], **Guojun Bu**[3], **Nelly Chuqui Owens**[1], **Sanket V. Rege**[1], **Gabriel Si**[1], **Ashim Ahuja**[1], **Donghui Zhu**[4], **Carol A. Miller**[5], **Julie A. Schneider**[6], **Manami Maeda**[7,8], **Takahiro Maeda**[7,8], **Tohru Sugawara**[9], **Justin K. Ichida**[9], and **Berislav V. Zlokovic**[1,†]

[1]Zilkha Neurogenetic Institute and Department of Physiology and Biophysics, Keck School of Medicine, University of Southern California, Los Angeles, CA 90033, USA

[2]Department of Neurological Surgery, University of California San Francisco, San Francisco, CA 94143, USA

[3]Department of Neuroscience, Mayo Clinic, Jacksonville, FL 32224, USA

[4]Department of Chemical, Biological and Bio–Engineering, North Carolina Agricultural and Technical State University, Greensboro, NC 27411, USA

[5]Department of Pathology, Keck School of Medicine, University of Southern California, Los Angeles, CA 90033, USA

[6]Alzheimer's Disease Center, Rush University Medical Center, Chicago, IL 60612, USA

[7]Division of Hematopoietic Stem Cell and Leukemia Research, Beckman Research Institute of the City of Hope, Duarte, CA 91010, USA

[8]Division of Hematology, Department of Medicine, Brigham and Women's Hospital, Harvard Medical School, Boston, MA 02115, USA

[9]Eli and Edythe Broad Center for Regenerative Medicine and Stem Cell Research, and Department of Stem Cell Biology and Regenerative Medicine, University of Southern California, 1425 San Pablo Street, BCC 307, Los Angeles, CA 90089, USA

Abstract

PICALM is highly validated genetic risk factor for Alzheimer's disease (AD). Here, we report that PICALM reductions in AD and murine brain endothelium correlate with amyloid–β (Aβ)

[†]**Address correspondence:** Berislav V. Zlokovic, M.D., Ph.D. Zilkha Neurogenetic Institute, Room: 101, 1501 San Pablo Street, Los Angeles, CA 90089, Phone: 323.442.2722 / Fax: 323.666.2184, zlokovic@usc.edu.

[10]These authors contributed equally to this work.

Authors Contributions

Z.Z., A.P.S. and Q.M. designed and performed experiments and analyzed data. M.R.H., P.K, K.K., N.C.O., S.V.R., G.S., A.A., and T.S. performed experiments. E.A.W. performed pilot experiments. A.R. performed *in vivo* microdialysis experiments. T.K. and G.B. contributed critical materials. D.Z. generated pilot data. C.A.M., J.A.S., M.M. and T.M. provided critical materials. J.K.I. designed iPSC study. B.V.Z. designed all experiments, analyzed data and wrote the manuscript.

pathology and cognitive impairment. Moreover, *Picalm* deficiency diminishes Aβ clearance across the murine blood–brain barrier (BBB) and accelerates Aβ pathology that is reversible by endothelial PICALM re–expression. Using human brain endothelial monolayer, we show that PICALM regulates PICALM/clathrin–dependent internalization of Aβ bound to the low density lipoprotein receptor related protein–1, a key Aβ clearance receptor, and guides Aβ trafficking to Rab5 and Rab11 leading to Aβ endothelial transcytosis and clearance. PICALM levels and Aβ clearance were reduced in AD–derived endothelial monolayers, which was reversible by adenoviral–mediated *PICALM* transfer. iPSC–derived human endothelial cells carrying the *rs3851179* protective allele exhibited higher PICALM levels and enhanced Aβ clearance. Thus, PICALM regulates Aβ BBB transcytosis and clearance that has implications for Aβ brain homeostasis and clearance therapy.

INTRODUCTION

PICALM, the gene encoding phosphatidylinositol binding clathrin assembly (PICALM) protein[1, 2], plays a key role in endocytosis and internalization of cell receptors[3–6]. PICALM also mediates intracellular trafficking of endocytic proteins[7, 8]. Several genome wide association studies have shown the association of *PICALM* with Alzheimer's disease (AD)[9–13], a neurological disorder characterized by neurovascular dysfunction, elevated amyloid β–peptide (Aβ), tau pathology and neuronal loss[14–16]. The role of PICALM in disease pathogenesis remains, however, elusive.

PICALM was originally postulated to affect disease by modifying trafficking of Aβ precursor protein (APP)[9]. Recent studies suggested that PICALM protects neurons from Aβ toxicity by reversing Aβ effects on clathrin–mediated endocytosis[6] and/or by directing APP transport to the terminal degradation pathway by autophagosomes which reduces Aβ production[17]. In contrast, viral–mediated silencing of PICALM in the hippocampal neurons in *APP*–overexpressing mice was shown to diminish Aβ production resulting in a moderate reduction in Aβ load[18]. Furthermore, PICALM influences Aβ42/total Aβ ratio in neurons through clathrin–mediated endocytosis of γ–secretase[19].

In addition to its neuronal functionality, PICALM is abundantly expressed in brain capillary endothelium[20, 21], a site of the blood–brain barrier (BBB) *in vivo*[14], which provides a major pathway for Aβ clearance from the brain into circulation[14, 22, 23]. Thus, PICALM is ideally situated to regulate the function of brain capillary endothelial receptors including receptors that mediate Aβ clearance such as the low density lipoprotein receptor related protein 1 (LRP1) which binds Aβ, and is a key Aβ clearance receptor at the BBB and vascular cells[22–27]. Therefore, we hypothesized that PICALM *i)* influences Aβ clearance across the BBB; and *ii)* at the molecular level, regulates the function of LRP1 in brain endothelial cells[22–24]. Our data suggest that endothelial PICALM plays a central role in Aβ clearance and transcytosis across the BBB, which is critical for regulation of Aβ levels and homeostasis in the brain.

RESULTS

PICALM reductions in brain endothelium in Alzheimer's disease

First, we show robust expression of PICALM in microvessels in aged control human brains without dementia by immunocytochemistry (Fig. 1a, left panels), immunoblotting (Fig. 1b–c) and double fluorescence immunostaining for PICALM and endothelial–specific *Lycopersicon esculentum* lectin (Fig. 1d, left panels; Supp. Fig. 1a, upper panels) indicating that ~65% of the endothelial cell surface area labeled with lectin is positive for PICALM in the hippocampus and cortex (Fig. 1e). PICALM levels in isolated cortical microvessels from control human brains were >1.7–fold higher than in capillary–depleted brain homogenates containing neurons and glia (Fig. 1b–c). In advanced AD (Braak stage V–VI) compared to controls (Braak stage I), PICALM levels were reduced in cerebral microvessels (Fig. 1a, right panels; Fig. 1b; Fig. 1d, right panels; Supplementary Fig. 1a, lower panels) by 55 to 65% as shown by immunoblotting (Fig. 1c) and double staining for PICALM and lectin, respectively (Fig. 1e). In contrast, immunostaining for PICALM and neuronal marker microtubule–associated protein 2 (MAP2) revealed a moderate increase in PICALM levels in neurons in advanced AD (Braak V–VI) compared to controls (Fig. 1d), consistent with a previous report[28]. When comparing 30 AD cases (Braak stage III–IV and V–VI) with 20 controls (Braak stage 0–I to III) (Supplementary Table 1a), we found that PICALM endothelial levels inversely correlated with Aβ load (Fig. 1f), Braak stage (Fig. 1g) and clinical dementia rating (Fig. 1h), and positively with mini–mental state exam scores (Fig. 1i). As in humans, PICALM levels in murine brain microvessels were >2–fold higher than in capillary–depleted brain homogenates (Supplementary Fig. 1a). Notably, elevated Aβ levels in APP–overexpressing $APP^{Sw/0}$ mice[29] or in endothelial cultures did not affect PICALM levels (Supplementary Fig. 1a–e), ruling out Aβ as a PICALM suppressor. Therefore, endothelial loss of PICALM in AD is associated with greater Aβ and AD pathology and worse cognitive impairment.

Diminished Aβ clearance in *Picalm*$^{+/-}$ mice

To address whether PICALM plays a role in Aβ clearance across the BBB *in vivo* and may contribute to worsening AD pathology, we next studied clearance of human Aβ40 and Aβ42 in *Picalm*$^{+/-}$ mice generated as shown in Supplementary Fig. 2a–b. Complete knockout of *Picalm* is embryonic lethal, but *Picalm*$^{+/-}$ mice develop normally and have normal blood glucose, hepatic and renal analyses (Supplementary Fig. 2a–n) and do not show behavioral changes within 9 months of age (Supplementary Fig. 2a–r). Compared to their littermate controls, *Picalm*$^{+/-}$ mice had ~70% lower levels of PICALM in brain microvessels and ~50% reduction in PICALM in capillary–depleted brain (Fig. 2a–b). Using an Aβ clearance assay[22, 23] and ELISA[27] we show that 3 month old *Picalm*$^{+/-}$ mice have 38% and 36% greater brain retention of Aβ40 and Aβ42, respectively, 30 minutes following intracerebral administration of human Aβ40 or Aβ42 (1 ng), when compared to controls (Fig. 2c). There was no difference in retention of inulin, an inert extracellular space marker frequently used to estimate brain interstitial fluid (ISF)–to–cerebrospinal fluid (CSF) bulk flow[22, 23] (Fig. 2c). Consistent with these results, *Picalm* deficiency diminished Aβ40 and Aβ42 efflux across the BBB by 41% and 61%, respectively (Fig. 2d; see Methods), but did not affect Aβ efflux via ISF compared to controls (Fig. 2e). We found 48% and 65% lower plasma levels

of Aβ40 and Aβ42, respectively, in *Picalm*$^{+/-}$ mice compared to control *Picalm*$^{+/+}$ mice (Fig. 2f), confirming impaired Aβ clearance from brain to blood.

Effects of *Picalm* deficiency and endothelial–specific rescue in *APP*$^{sw/0}$ mice

To address whether *Picalm* deficiency can influence Aβ pathology, we crossed transgenic *APP*$^{sw/0}$ mice which develop Aβ elevation and correlative memory deficits[29] with *Picalm*$^{+/-}$ mice. *APP*$^{sw/0}$; *Picalm*$^{+/-}$ mice had ~70% lower levels of PICALM in microvessels and ~50% reduction in PICALM in capillary–depleted brain compared to their respective littermate controls (Supplementary Fig. 3a–b). Using hippocampal *in vivo* microdialysis[27] (see Methods), we show a significant 2.4 and 2.5–fold increase in the steady–state levels of soluble Aβ40 and Aβ42 in brain ISF of 3 month old *APP*$^{sw/0}$; *Picalm*$^{+/-}$ mice compared to age–matched littermate controls, respectively (Fig. 3a–b). After intraperitoneal injection of the γ–secretase inhibitor Compound E, the half–life of Aβ40 and Aβ42 in brain ISF[27] was increased in *APP*$^{sw/0}$; *Picalm*$^{+/-}$ mice compared to *APP*$^{sw/0}$; *Picalm*$^{+/+}$ controls from 1.2 to 1.9 hours, and 1.4 to 2.5 hours, respectively (Fig. 3c), suggesting that the increase of ISF Aβ levels was due to diminished Aβ clearance. The increase in Aβ ISF levels preceded Aβ and amyloid deposition. Deposits were absent in 3–month–old *APP*$^{sw/0}$; *Picalm*$^{+/-}$ mice (Fig. 3d), but began to accumulate at 6 months of age as shown by the increase in Aβ load in the hippocampus and cortex and accelerated development of cerebral amyloid angiopathy (Supplementary Fig. 3a–d). Importantly, 9 month old *APP*$^{sw/0}$*; Picalm*$^{+/-}$ mice had a significant 3.5–4–fold increase in Aβ load in the cortex and hippocampus (Fig. 3e–f) associated with worse performance in behavioral tests including nest construction, burrowing, novel object location and novel object recognition (Fig. 3g–i) compared to age–matched littermate controls.

To specifically address the role of endothelial PICALM in transvascular Aβ clearance we performed a rescue experiment. We generated *APP*$^{sw/0}$*; Picalm*$^{+/-}$*; Tie2–Cre* line and an adeno–associated viral (*AAV*)–*Flex–Picalm* construct for delivery of a Cre–dependent expression cassette (*Flex–Picalm*) specifically to brain endothelium in the hippocampus (Fig. 4a). After administration of *AAV–Flex–Tdtomato* into the hippocampus of 5 month old *APP*$^{sw/0}$; *Picalm*$^{+/-}$; *Tie2–Cre* mice, >50% of lectin–positive endothelial vascular profiles expressed Tie2–Cre–dependent Tdtomato (red) (Supplementary Fig. 4a). Co–injection of *AAV–Flex–Tdtomato* and *AAV–Synapsin–GFP* revealed that <3% of hippocampal neurons express Tdtomato. Together these data confirm Tie2–Cre–dependent endothelial–specific expression of transgene and minimal leakage in neurons. Similar results were obtained after administration of *AAV–Flex–Picalm* into the hippocampus of 5 month old *APP*$^{sw/0}$; *Picalm*$^{+/-}$; *Tie2–Cre* mice showing Tie2–Cre–dependent Flag–PICALM expression in >50% lectin–positive endothelial vascular profiles, and negligible expression in neurons after co–injection of *AAV–Flex–Picalm* and *AAV–Synapsin–GFP* (Fig. 4b). PICALM re–expression in endothelium of *APP*$^{sw/0}$*; Picalm*$^{+/-}$*;Tie2–Cre* mice after *AAV–Flex–Picalm* administration in the ipsilateral hippocampus diminished Aβ load, Aβ40 and Aβ42 levels by 63%, 46% and 37% respectively, compared to the contralateral hippocampus injected with *AAV–Flex* (control) virus (Fig. 4c–e; Supplementary Fig. 4a). Moreover, bilateral administration of *AAV–Flex–Picalm* in the left and right hippocampus improved behavior in *APP*$^{sw/0}$*; Picalm*$^{+/-}$*;Tie2–Cre* mice compared to *AAV–Flex* (control) as shown in a separate

group of mice (Fig. 4f–g). These data strongly support our hypothesis that brain endothelial PICALM has a central role in regulating Aβ clearance from the brain by controlling its efflux at the BBB.

Neither *Picalm*$^{+/-}$ nor *APP*$^{sw/0}$; *Picalm* $^{+/-}$ mice compared to their respective controls had changes in Aβ production and processing[15, 16], brain microvascular expression of major Aβ transporters including P–glycoprotein, LRP1 and RAGE[14], or Aβ degrading enzymes including neprilysin and insulin–degrading enzyme[16] (Supplementary Fig. 5), which make these mechanisms unlikely contributors to decreased Aβ clearance and/or increased Aβ accumulation.

PICALM/clathrin–dependent endocytosis of Aβ–LRP1 complex by endothelial cells

To elucidate the molecular mechanism(s) underlying PICALM regulation of Aβ clearance across the BBB we studied Aβ internalization and trafficking in primary human brain endothelial cells (BEC) and subsequently in an *in vitro* model of the BBB[30]. First, we show that Aβ40 binds to the cell surface LRP1 in BEC at 4 °C as reported[14, 23] (Supplementary Fig. 6a; see Methods and Supplementary Table 1a – control donors), and that 6–carboxyfluorescein–labeled (FAM)–Aβ40–LRP1 complex colocalizes rapidly (≤ 30 s) with PICALM (Fig. 5a, d) and proteins responsible for PICALM/clathrin–dependent internalization of ligands[2, 5] at 37 °C – including clathrin heavy chain (CHC) (Fig. 5b, c, d) and clathrin adaptor protein α–adaptin (AP–2) (Supplementary Fig. 6a). Similar to Aβ40, FAM–Aβ42, but not scrambled FAM–Aβ42 (Supplementary Fig. 6a–d), led to a rapid increase in colocalized Aβ–LRP1/PICALM puncta. Rapid recruitment of PICALM and the clathrin endocytotic apparatus to LRP1 has been confirmed by co–immunoprecipitation analysis 30 s after Aβ40 treatment at 1 nM – a concentration corresponding to Aβ40 levels in the CSF[14, 16] (Fig. 5e). In contrast to PICALM that remains associated with LRP1 over longer periods of time, CHC and AP–2 dissociate early from LRP1 (Fig. 5e) consistent with rapid uncoating of clathrin from internalized vesicles[5]. siRNA inhibition of PICALM or CHC inhibited Aβ40–induced LRP1 internalization (Fig. 5f) suggesting that endocytosis of Aβ–LRP1 complex requires both PICALM and clathrin.

To further understand PICALM interaction with LRP1, we studied binding of human recombinant PICALM to human recombinant glutathione S–transferase (GST) tagged LRP1 C–terminus fusion protein which indicated direct binding of PICALM to LRP1 C–terminus (Fig. 5g), but not to GST (Supplementary Fig. 6a; control assay). Although, this experiment was carried out in the absence of cells, we cannot rule out a possibility that in the cellular milieu some intermediary proteins can facilitate and/or influence PICALM binding to LRP1. Using co–immunoprecipitation analysis after transfection of cells with PICALM and various mutants of the C–terminus LRP1 cytoplasmic tail[31], we found that PICALM binding to LRP1 requires *YXXL* motif (Fig. 5h–i).

To determine specificity of Aβ as a ligand that enhances the binding of PICALM to the cytoplasmic tail of LRP1, we studied other LRP1 ligands including apolipoprotein E (apoE) and activated α2–macroglobulin (α2M*). Incubation of BEC with astrocyte–derived lipidated apoE3, apoE4[32] and α2M* did not result in a rapid binding of PICALM to LRP1, whereas Aβ40 binding to apoE3, apoE4 and α2M* inhibited PICALM binding to LRP1

(Supplementary Fig. 7a). Consistent with these data, binding of Aβ40 to apoE4, apoE3 and α2M* inhibited Aβ40–induced internalization of LRP1 (Supplementary Fig. 7a–c). Collectively, these data suggest that binding of Aβ to the ectodomain of LRP1 has a unique conformational effect on its cytoplasmatic C–terminus tail enhancing the binding of PICALM, which initiates PICALM/clathrin–dependent endocytosis of Aβ–LRP1 complex.

PICALM associates with LRP1 during Aβ transcytosis across endothelial monolayer

We next used an *in vitro* model of the BBB[30] to study the role of PICALM in Aβ transport across fully confluent (> 97%) human brain endothelial monolayer co–cultured with pericyte–conditioned medium, as pericytes critically influence the BBB properties[33–35]. The endothelial monolayer had a typical cobblestone pattern of the zonula occludens 1 (ZO–1) tight junction protein and a cortical distribution of the F–actin cytoskeleton, and expressed PICALM (Fig. 6a). A transmonolayer electrical resistance (TEER) of ~280 ohms·cm^2 and a low paracellular permeability constant (P) of ~ 1.21×10^{-6} cm·s^{-1} determined for dextran (MW=40 kDa), a metabolically inert polar molecule, confirmed formation of the barrier.

To ascertain whether our endothelial monolayer model is suitable for Aβ transport studies, we determined cell polarity for two key Aβ transporters, LRP1 and the receptor for advanced glycation end products (RAGE) that are expressed in brain endothelium *in vivo* mainly at the abluminal (basolateral) and luminal (apical) side, respectively[14], as confirmed by signal intensity profile analysis across capillary lumens in human brain (Supplementary Fig. 8a–b). In agreement with *in vivo* findings, LRP1 and RAGE colocalized chiefly towards the basolateral and apical membrane of the endothelial monolayer, respectively (Supplementary Fig. 8a). PICALM associated with LRP1–Aβ40 complex in the endothelial monolayer rapidly after Aβ application to the basolateral membrane (Fig. 6b), similar as in BEC cultures (Fig. 5a, d–e).

The proximity ligation assay (PLA)[32, 36] confirmed that PICALM associates rapidly with LRP1 in the endothelial monolayer after Aβ40 (1 nM) addition to the basolateral membrane with a peak at 30 s and a plateau over 4 min (Fig. 6c–d). In contrast, LRP1–clathrin association peaked within 30 s and was followed by a sharp decline within 1 min (Fig. 6d) consistent with coimmunoprecipitation data showing rapid dissociation of clatrhin from internalized LRP1 (Fig. 5e).

To further study the roles of LRP1, PICALM and CHC in Aβ internalization at the basolateral endothelial membrane and the basolateral–to–apical transendothelial transport (transcytosis), we utilized siRNA silencing. Aβ40 (1 nM) internalization was rapid with a $t_{1/2}$ of ~17 s (Fig. 6e) as reported for LRP1–mediated endocytosis[31]. siRNA inhibition of *LRP1*, *PICALM* or *CHC* substantially diminished Aβ internalization by >90% within 1 min compared to control si.*Scrambled* RNA (Fig. 6e), suggesting that all three molecules are essential for Aβ internalization. Basolateral–to–apical transcytosis of Aβ40 (1 nM) [determined by Aβ40 ELISA measurements in the basolateral and apical chambers corrected for paracellular diffusion by subtracting diffusion values of inulin, a metabolically inert polar molecule; see Methods] was inhibited by the receptor–associated protein (RAP) and LRP1–specific antibodies, but not other LDL receptors–specific antibodies (Supplementary Fig. 8a). si.*LRP1*, but not si.*Scrambled* RNA, also inhibited Aβ40 basolateral–to–apical

transendothelial transport (Supplementary Fig. 8a). These data confirm that Aβ binding to LRP1 initiates Aβ clearance at the basolateral membrane of the monolayer, as previously suggested[14, 22, 23], and that LRP1 is required for Aβ transcytosis across the monolayer. As expected, silencing *PICALM* and *CHC* inhibited Aβ40 transcytosis across the monolayer by approximately 85% as shown within 30 min of the unidirectional basolateral–to–apical transendothelial Aβ transport (Fig. 6f–g). Within 5 min of Aβ application to the basolateral membrane of the endothelial monolayer, Aβ–LRP1 internalized complex was already found nearby the apical membrane of the monolayer (Supplementary Fig. 9a) confirming basolateral–to–apical trans–endothelial transport.

PICALM guides Aβ trafficking to Rab 5 and Rab 11 leading to Aβ endothelial transcytosis

Since PICALM remains associated with LRP1 over longer periods of time in contrast to CHC and AP–2 that dissociate rapidly from internalized Aβ–LRP1 vesicles (Fig. 5e; Fig. 6d), we next traced intracellular trafficking of PICALM and Aβ–LRP1 using molecular markers for different steps of the endosomal pathway. Because Rab5 and Rab7 regulate Aβ endosomal trafficking in neurons[37], we asked whether PICALM interacts with Rab GTPases[38] following Aβ–LRP1 internalization. Using subconfluent endothelial cultures, we show that PICALM and Aβ40–LRP1 complex colocalize with Rab5– and EEA1–positive early endosomes[5] within 2 min of Aβ40 (1 nM) treatment (Fig. 7a, d; Supplementary Fig. 10a–b), but not with Rab7, a GTPase that directs fusion of late endosomes with lysosomes[38] leading to degradation of ligands[39] (Fig. 7b), or the lysosomal–specific marker LAMP1[38] (Supplementary Fig. 10c). Rather, PICALM colocalized with Rab11 (Fig. 7c), a GTPase which regulates recycling of vesicles controlling transcytosis[40–42] and exocytosis[43] of ligands. Aβ42 also colocalized with Rab5 and Rab11 (Supplementary Fig. 11a–b). In the absence of Aβ, PICALM minimally colocalized with Rab5, Rab7 and/or Rab11 (Supplementary Fig. 11c–e). These data suggest that PICALM likely regulates trans–endothelial Aβ trafficking by shunting Aβ away from a degradation pathway towards a transcytotic pathway, consistent with previously demonstrated clathrin–independent functions of PICALM[7, 8, 17]. Interestingly, the peak co–localization between PICALM and Rab5 (Fig. 7a, d) was somewhat higher than the peak co–localization between PICALM and Rab11 (Fig. 7c, d), suggesting that transfer of PICALM–containing endocytic vesicles from Rab5 to Rab11 could potentially be a rate–limiting step in Aβ transcytosis.

Using an *in vitro* endothelial monolayer model of the BBB, we next show that FAM–Aβ40 associates with Rab5 and Rab11 in the endothelium within 2 and 4 min of its application to the basolateral membrane, respectively (Fig. 7e–f). PICALM–Rab11 association peaked at 4 min of incubation with Aβ40 at the basolateral membrane and remained at a ‘plateau’ at 5 min (Fig. 7g–h), whereas PICALM–Rab5 association peaked at 2 min and declined within 3–4 min (Fig. 7h), as shown by PLA analysis. PICALM–Rab7 association was undetectable (Fig. 7h). PICALM interaction with LRP1, Rab5 and Rab11 at different time points after Aβ40 treatment has been corroborated by coimmunoprecipitation analysis (Fig. 7i).

Consistent with findings showing that Rab5 is necessary for the biogenesis of early and late endosomes[44], dominant negative Rab5–S34N mutant (see Methods) inhibited Aβ transcytosis by >85% as compared to EGFP control (Fig. 7j–k). Dominant negative Rab11–

S25N mutant, but not Rab7–T22N mutant, also inhibited unidirectional Aβ40 basolateral–to–apical transport by 75% (Fig. 7j–k). These data suggest that Rab11 likely controls later stages of Aβ transcytosis across the monolayer consistent with findings showing that Rab11 regulates trafficking of vesicles controlling transcytosis[40–42] and exocytosis[43] of ligands. siRNA inhibition of Rab11b, but not Rab11a, blocked Aβ transcytosis (Supplementary Fig. 9a) consistent with findings that Rab11b is the major Rab11 isoform in brain endothelium, whereas Rab11a is a major isoform in epithelial cells[40–42] as confirmed in this study (Supplementary Fig. 9a).

Importantly, siRNA knockdown of *PICALM* inhibited by 80% and 95% Rab5 and Rab11 GTPase activity in the endothelial monolayers treated with Aβ40, respectively (Fig. 7l–m), demonstrating that PICALM binding to Rab5 and Rab11 is critical for maintaining Rab5 and Rab11 GTPase activity during endosomal trafficking of Aβ. Consistent with findings showing that PICALM does not direct Aβ to lysosomes for degradation, Aβ was >95% intact within 30 min of unidirectional transcytosis and clearance across the monolayer (Supplementary Fig. 9a), as reported[23]. Collectively, our data indicate that PICALM controls the transcytotic pathway mediating Aβ clearance across the BBB.

PICALM levels and Aβ clearance by endothelial monolayers from Alzheimer's patients

To determine the role of PICALM in Aβ clearance in AD brain endothelium (Supplementary Table 1a), we studied Aβ transcytosis across AD–derived endothelial monolayers co–cultured with pericyte conditioned media. The AD endothelial monolayers had a normal cobblestone pattern, TEER values and paracellular permeability (Supplementary Fig. 12a–c). Consistent with diminished PICALM levels in AD brain endothelium *in situ* and in brain capillaries (Fig. 1), PICALM mRNA and protein levels were reduced by 34–35% in cultured AD BEC (Fig 8a) resulting in ~50% diminished basolateral–to–apical transcytosis of Aβ across AD–derived endothelial monolayers compared to age–matched controls (Fig. 8b). LRP1 levels are also reduced in AD brain endothelium[22, 23], whereas AP–2, CHC, Rab5 and Rab11b expression is comparable to controls (not shown). Adenoviral–mediated transfer of *PICALM* compared to *GFP* control (Supplementary Fig. 12d) substantially improved Aβ transcytosis by 63%, whereas co–transfer of *PICALM* and *LRP1* mini–gene[32] improved Aβ transport by 89% (Fig. 8b), suggesting that PICALM can be therapeutically targeted.

Aβ clearance by iPSC–derived endothelium carrying the *rs3851179 PICALM* variants

All AD–associated single–nucleotide polymorphisms (SNPs) in PICALM are located upstream to the coding region of the gene, and no mutation in the PICALM protein has been identified to influence AD risk[9–13]. Some AD–associated *PICALM* SNPs have been suggested, however, to influence PICALM expression, as for example rs659023 variants in peripheral blood mononuclear cells[45]. To address whether certain PICALM variants can influence PICALM expression and Aβ clearance in endothelial cells, we focused on highly validated and replicated *rs3851179 PICALM* variants whose $rs3851179^{A}$ allele compared to $rs3851179^{G}$ allele is associated with a lower risk of AD[9, 10, 12]. To test the phenotypic differences between the minor protective $rs3851179^{A}$ allele and the major non–protective $rs3851179^{G}$ allele in human endothelial cells, we utilized inducible pluripotent stem cells (iPSCs) technology. The iPSCs were generated from lymphoblasts from Coriell using the

episomal plasmids and encoding factors as we described[46]. We next used CRISPR/Cas9 genome editing[47] to generate the isogenic homozygous iPSC lines for the two homozygous allelic variants (Fig. 8c–e) followed by direct differentiation to generate bona fide endothelial cells[48] and endothelial monolayers (Fig. 8f–g; for details see Methods). iPSC–derived endothelial cells carrying the protective *rs3851179*^{A} allele compared to the non–protective *rs3851179*^{G} allele had 72–78% higher expression levels of *PICALM* mRNA and protein (Fig. 8h) and 120% higher Aβ clearance (Fig. 8i).

DISCUSSION

We show that PICALM reductions in brain endothelium in AD correlate with Aβ and AD neuropathology and cognitive impairment, whereas reduction and re–expression of PICALM in endothelial cells influence Aβ clearance at the BBB and Aβ deposition in the mouse brain and phenotypic manifestations of behavior in mice. At a molecular level, using an *in vitro* endothelial monolayer that approximates BBB we show that i) Aβ binding to the ectodomain of LRP1 enhances the binding of PICALM which initiates PICALM/clathrin–dependent endocytosis of Aβ–LRP1 complex; and ii) PICALM remains associated with LRP1 after Aβ internalization and directs Aβ trafficking to Rab5 and Rab11 leading to Aβ transcytosis (Supplementary Fig. 13). PICALM levels and Aβ clearance are greatly reduced in AD–derived endothelial monolayers, which was reversible by adenoviral–mediated *PICALM* transfer. Using iPSC–derived human endothelial cells carrying *rs3851179* PICALM variants, we show that the protective *rs3851179* allele leads to a higher *PICALM* expression and enhanced Aβ clearance by endothelial cells.

AAV8 viral–mediated silencing of neuronal PICALM in the hippocampus moderately reduced Aβ production in *APP/PS1* mice[18], but whether a moderate reduction in Aβ load as seen in this study is beneficial for neurons after inactivation of PICALM is unclear as PICALM also protects neurons against Aβ toxicity[6]. Mice with PICALM loss–of–function allele as used in our study develop accelerated Aβ accumulation and have lower behavioral test performance compared to controls, raising the possibility that in models of global *Picalm* deficiency, where PICALM is deleted in multiple cell populations (e.g., endothelial cells, neurons), the effect of *Picalm* loss from endothelium causing faulty Aβ vascular clearance may override the discrepant reduction in Aβ secretion from neurons[18]. Future studies in transgenic mice with inducible PICALM deletion in neurons should address its Aβ–independent effects, particularly as PICALM regulates axonal growth[49] and turnover of synaptic vesicles and receptors[50].

Our data surprisingly revealed that PICALM guides intracellular trafficking of Aβ–LRP1 to Rab5 and Rab11 leading to Aβ transcytosis across endothelial monolayer, which does not require clathrin beyond the early internalization steps. These findings are consistent with previously demonstrated clathrin–independent functions of PICALM in trafficking of endocytic proteins[7, 8, 17].

At present, little is known about upstream regulators of PICALM expression. Using *APP*–overexpressing mice and brain endothelial cultures we show that elevated Aβ does not suppress PICALM in endothelium. Multiple factors in AD including turbulent capillary

flow, oxidant stress, hypoxia or inflammation can affect gene expression in endothelial cells[14], potentially leading to PICALM reductions in endothelium. Identifying inhibitors of PICALM expression in AD endothelium would require, however, future studies interrogating multiple genetic, environmental and local brain factors.

Consistent with a concept that some AD–associated *PICALM* SNPs may influence PICALM expression[21, 45] using iPSCs technology we show that the protective *rs3851179* allele has a major effect on PICALM expression and Aβ clearance by endothelial cells. Future studies correlating PICALM levels in endothelium in human brain tissue with the genotype of patients in large cohorts of control and AD patients should provide additional information how different PICALM SNPs relate to each other and/or to other genes that influence Aβ clearance, as for example apoE or clusterin[16], and interrogate the roles of vascular risk factors, environment and lifestyle.

Collectively, our findings suggest that PICALM controls Aβ transport across the BBB and clearance from brain, and is therefore an important novel therapeutic target for Aβ clearance therapy.

ONLINE METHODS

Reagents

We used the following: 6-carboxyfluorescein-labeled (FAM)-Aβ40 (catalog # 23514), FAM-Aβ42 (catalog # 23526) and scrambled FAM-Aβ42 (catalog # 60892) (Anaspec, Fermont, CA); unlabeled Aβ40 and Aβ42 (Biopeptide, San Diego, CA); anti-HA monoclonal antibody (catalog # H9658, 1:5000, western blot) and anti-Flag monoclonal antibody (catalog # F3165, 1:5000 for western blot, 1:200 for co-IP) (Sigma); anti-Clathrin Heavy Chain monoclonal antibody (Thermo Scientific, catalog # MA1-065, 1:2000 for western blot, 1:500 for immunostaining); rabbit monoclonal anti-LRP1 antibody (EPR3724) (Abcam, catalog # ab92544, 1:5000 for western blot; 1:200 for immunostaining); rabbit polyclonal anti-PICALM antibody (Sigma, catalog # HPA019061, 1:5000 for western blot, 1:200 for immunostaining); goat polyclonal anti-PICALM antibody from Santa Cruz (Catalog # SC-6433, 1:2000 for western blot, 1:100 for immunostaining); rabbit polyclonal anti-EEA1 (catalog # 2411), Rab5 (catalog # 3547), Rab7 (catalog # 9367), Rab11 (catalog # 5589), Rab11a (catalog # 2413), Rab11b (catalog # 2414) (Cell Signaling, 1:2000 for western blot; 1:100 for immunostaining); mouse monoclonal anti-LAMP1 antibody (H4A3) (Abcam, catalog # ab25630, 1:200 for immunostaining); rabbit polyclonal anti-AP2 alpha antibody (Abcam, catalog # ab116289, 1:2000 for western blot); Rab5-S34N (catalog # 28045), Rab7-T22N (catalog # 12660) and Rab11-S25N (catalog # 12680) (Addgene). Human RAB11b gene was cloned from human adult brain cDNA library (Invitrogen, catalog # D8030) by polymerase chain reaction (PCR) and sub-cloned into pEGFP-C1 vector (Clontech) using BAMH1 site. RAB11b-S25N mutant was generated by site-directed mutagenesis using GeneArt mutagenesis system (Invitrogen, catalog # A13282). The constructs carrying the membrane-containing minireceptor of LRP1 and its mutants were from Dr. Bu's laboratory[26]. Human PICALM cDNA clone (Openbiosystem, clone ID: 5112878) was subcloned into pCDNA5-Flag vector or pAEasy-1 vector (Agilent, Catalog #24005) using pShuttle-CMV vector (Agilent, Catalog #24007) for viral production.

Adenoviral vector carrying LRP1 minigene (Ad.*mLRP1*) was prepared as we previously reported[32]. We also used a complete EDTA free cocktail of protease inhibitors and phosphatase inhibitors (Roche Applied Sciences, Indianapolis, IN); human recombinant RAP (EMD Biosciences, Inc., San Diego, CA); monoclonal mouse antibody P2-1 specific for human APP (1:1000, 1 mg/ml) and 22C11 that recognizes mouse and human APP (1:100, 0.5 mg/ml) (Chemicon International, Temecula, CA);RAGE-specific IgG (1:500, 1 mg/ml)[24]; rabbit ant-NICD antibody (Millipore, catalog #07-1232) and rabbit polyclonal anti-human Aβ (Cell Signaling Technology, catalog #8243; 1:200). Secondary antibodies were: Alexa 488-conjugated donkey anti-rabbit (Invitrogen; A11008; 1:200), Alexa 568-conjugated donkey anti-goat (Invitrogen; A11057; 1:200), Alexa 647-conjugated donkey anti-goat (Invitrogen; A21447; 1:200), Alexa 488-conjugated donkey anti-mouse (Invitrogen; A21202; 1:200), Alexa 647-conjugated donkey anti-mouse (Invitrogen; A31571; 1:200); HRP-conjugated donkey anti-mouse (Invitrogen; A16011; 1:5000), HRP-conjugated donkey anti-goat (Invitrogen; A16005; 1:5000), and HRP-conjugated donkey anti-rabbit (Invitrogen; A16029; 1:5000). Nuclei were stained with Hoechst 33342 (Invitrogen; 1:10,000).

Human postmortem studies

Tissue samples—Post-mortem paraffin embedded human frontal cortex and hippocampus samples were obtained from the Rush University Medical Center and the University of Southern California. Informed consent was obtained and the study approved by the Institutional Review Board of Rush University Medical Center and the University of Southern California. All autopsy cases underwent neuropathological evaluation of AD including assignment of Braak stages. Aged subjects that did not carry diagnosis of AD or another neurodegenerative disease and showed neuropathological findings within the normal range for age were used as age-matched controls. MMSE and CDR information were available for most but not all individuals. Frozen brain tissue specimens were from the prefrontal cortical grey matter (Brodmann area 9, 10) and were snap-frozen and stored at −80°C. A total of 20 controls and 30 AD individuals were used for histopathological analyses. The demographic information of all cases is provided in Supplementary Table 1a.

Histopathological analyses—Heat-induced antigen retrieval was performed following Dako's protocol. For immunohistochemistry analysis of PICALM or Aβ, ImmPRESS™ Polymer-Based Immunohistochemistry Reagents (Vector Laboratories) were used for visualization. For immunofluorescence analysis, species-specific fluorochrome-conjugated secondary antibodies were incubated for 1 h at room temperature, and blood vessels were stained by Dylight 488-conjugated *L. esculentum* lectin for 1 h at room temperature. All slices were scanned using Zeiss 510 confocal microscope with Zeiss Apochromat water immersion objectives (Carl Zeiss MicroImaging Inc., Thornwood, NY, USA).

Isolation of cerebral microvessels and microvessel-depleted brain—These were isolated from frozen human cortical tissue samples using dextran gradient centrifugation followed by sequential cell-strainer filtration as we have previously described[51, 52].

Animals

All procedures were approved by the Institutional Animal Care and Use Committee at the University of Southern California with National Institutes of Health guidelines. All animals were included in the study. Animals of both sexes 3, 6 and 9 month old were used in the experiments. All animals were randomized for their genotype information. All experiments were blinded; the operators responsible for the experimental procedures and data analysis were blinded and unaware of group allocation throughout the experiments.

Generation of Picalm$^{+/-}$ mice—Gene-targeting strategy for *Picalm* mutant strains is described in Supplementary Fig. 2. Genotyping of the mutant mice was performed by PCR of tail DNA with the following primers; PicalmFW CATAAGCTAAGATTTCCCCTGTCACA and PicalmRV CCACCATGTAGGGTCTAAAG.

Generation of APP$^{sw/0}$; Picalm$^{+/-}$ mice—*APP*$^{sw/0}$ mice expressing human APP transgene with the K670M/N671L (Swedish) double-mutation under control of the hamster prion promoter[23, 27] were crossed with *Picalm*$^{+/-}$ mice to generate *Picalm*-deficient *APP*$^{sw/0}$; *Picalm*$^{+/-}$ mice and their corresponding littermate controls. All experiments were performed using age-matched littermates.

In vivo BBB efflux

CNS clearance of unlabeled synthetic human Aβ40 and Aβ42 peptides was determined simultaneously with ^{14}C-inulin (reference marker) in male *Picalm*$^{+/-}$ mice and littermate controls at 3 months of age using a procedure as we described[22, 23]. Brain and blood were sampled 30 min after Aβ injection and prepared for Aβ40 or Aβ42 ELISA[27] and ^{14}C-radioactivity analysis, as described[22, 23, 25, 53]. The percentage of Aβ40 or ^{14}C-radioactivity remaining in the brain after microinjection was determined as % recovery in brain = 100 × (N_b/N_i), where Nb is the amount of Aβ40 or ^{14}C-inulin remaining in the brain at the end of the experiment and N_i is the amount of Aβ40 or ^{14}C-inulin simultaneously injected into the brain ISF, i.e., the amount of intact Aβ40 based on ELISA and the d.p.m. for ^{14}C-inulin, respectively. The percentage of Aβ cleared through the BBB was calculated as [(1 − N_b(Aβ)/N_i(Aβ)) − (1 − N_b(inulin)/N_i(inulin))] × 100, using a standard time of 30 min.

In vivo microdialysis and ISF Aβ half-life determination

In vivo microdialysis was used to measure soluble Aβ40 and Aβ42 steady state levels in the hippocampus of awake, freely moving 3 month old *APP*$^{sw/0}$; *Picalm*$^{+/+}$ and *APP*$^{sw/0}$; *Picalm*$^{+/-}$ mice, as we recently described in detail[27]. Microdialysates were collected every 60 min into polypropylene tubes in a refrigerated fraction collector (Havard Apparatus). A stable baseline ISF Aβ40 and Aβ42 concentrations were obtained within 4 h followed by an i.p. injection of compound E (20 mg/kg, Millipore)[27]. The $t_{1/2}$ of Aβ was calculated in GraphPad Prism 5.0 software using the slope (k') of the linear regression that included all fractions between drug delivery and when Aβ concentrations plateau ($t_{1/2}$ = 0.693/k, where k = 2.303k')[27].

Biochemical analyses

Aβ40- and Aβ42-specific ELISA—Human-specific ELISA kits (Invitrogen) were used, as we described[27].

Measurement of sAPP-β levels and β-secretase activity—sAPP-β levels in brain of *APP$^{sw/0}$; Picalm$^{+/+}$* and *APP$^{sw/0}$; Picalm$^{+/-}$* mice were measured by ELISA kit (Covance) and β-secretase activity was determined using a β-secretase activity kit (Abcam).

Western Blotting—All samples were lysed in RIPA buffer, subjected to SDS-Page gel electrophoresis and transferred to a nitrocellulose membrane. Membranes were blocked with 5% milk, incubated with primary antibody, incubated with the appropriate HRP-conjugated secondary antibody, treated with Immobilon Western ECL detection buffers (Millipore), exposed to CL-XPosure film (Thermo Scientific) and developed in a X-OMAT 3000 RA film processor (Kodak, Rochester, NY), or ChemiDoc XRS system from Bio-Rad.

Tissue staining

Mice anesthetized as described above were transcardially perfused with PBS containing 5 U/ml heparin followed by 4% paraformaldehyde. OCT-embedded frozen brain tissue was cryosectioned at a thickness of 14–18 μm. All images were taken with a Zeiss 510 confocal microscopy or using the BZ 9000 all-in-one Fluorescence Microscope from Keyence (Osaka, Japan), and analyzed using NIH Image J software.

Behavioral analyses

Novel object location and recognition tests, nest construction test and burrowing test were performed as we reported[24, 32].

Endothelial specific rescue of PICALM deficiency

Endothelial specific rescue of PICALM was achieved by adeno-associated viral delivery of a Cre-dependent expression cassette (*Flex-Picalm*) to 5 month old *APP$^{sw/0}$*; *Picalm$^{+/-}$*; *Tie2-Cre* mice. The strategy was first validated with *AAV-Flex-tdTomato* virus (100 nl, 5x10^{12} GC/ml) and *AAV-synapsin-GFP* virus (20 nl, 5x10^{12} GC/ml) that were injected simultaneously into the hippocampus. *AAV-Flex-Picalm* construct was generated by cloning the coding region of mouse *Picalm* gene into the *pAAV-FLEX-tdTomato* (Addgene, Plasmid #28306) to replace the *tdTomato*. *AAV-Flex-Picalm* viruses were packaged by Penn Vector Core (6x10^{12} GC/ml) and 100 nl was used for each injection. The HBD mutant AAV-DJ/8 serotype (Cell Biolabs) was chosen for its high in vivo transduction efficiency and vascular tropism[54].

Viral injections—Surgical procedures were performed under general anesthesia with isoflurane (1–2%) using the SomnoSuite Small Animal Anesthesia System (Kent Scientific, CO) with rectal temperature monitored.

Primary human brain endothelial cell cultures

Isolation and characterization—We isolated and characterized brain endothelial cells (BEC) from rapid brain autopsies from the frontal cortex (area 9/10) from neurologically intact age-matched controls and AD patients as we previously described[24, 25, 55]. For clinical and neuropathological characteristics of donors please see below, and Supplementary Table 1a. BEC were > 98% pure, as measured by staining for the endothelial cell specific markers Von Willebrand Factor (vWF) and CD105, and negative immunostaining for the glial fibrillar acidic protein (astrocytes), CD11b (macrophage/microglia), smooth muscle cell α-actin (SMA) and platelet-derived growth factor receptor β and CD13 (pericytes). Early passage P2-P4 cultures were used throughout the study.

BEC cultures—All experiments were performed on at least three primary isolates using three different cultures from each isolate. For imaging and quantification analysis at least 20 cells from 5 different randomly selected fields in each culture (replicate) were selected.

LRP1 internalization assay—The cells were incubated with Aβ or other ligands for 15 min at 4°C for binding, washed with ice-cold Hank's Balanced Salt Solution three times, and then switched to 37°C water bath to initialize the internalization of LRP1. The fluorescence intensity of surface LRP1 staining was quantified using ImageJ software, and compared to the 4°C condition.

In vitro PICALM binding to LRP1—Recombinant human PICALM protein (Transcript variant 1, 70.6 kDa) was purchased from Origene (Catalog #TP313791). The *LRP1* C-terminal sequence (312 nucleotides) was cloned from the Human Brain cDNA library by PCR and sub-cloned into pGEX-4T1 vector using BamH1 and Not1 sites. GST and GST tagged LRP1 C-terminus fusion protein (330 amino acids) were produced in BL21 *E. coli* cells and purified with glutathione magnetic beads (Pierce, Catalog # 88822) following manufacturer's procedure. *In vitro* binding assay was performed using 5 μg of PICALM and 2 μg of GST fusion proteins (on the beads) in *Tris*-buffered saline at room temperature for 1 hour, and eluted with 25 mM glutathione.

HEK 293T cells—HEK 293T cells (ATCC, Manassas, VA) were cultured in high glucose DMEM medium supplemented with 10% FBS and penicillin (100 U/ml) and streptomycin (100 μg/ml) (Invitrogen) at 37°C with 5% CO_2. For transfection, 60~70% confluent cells in 10 cm plates were transfected with 20 μg of maxi-prepped plasmid DNA using Lipofectamine LTX.

In vitro model of the BBB—A single monolayer of fully confluent (> 97%) human BEC was produced by plating 5×10^5 cells/cm^2 in the upper chamber of a 6-well or 24-well tissue culture inserts (BD BioCoat, Catalog # 356408) pre-coated with rat tail collagen I and fibronectin, as we reported[20]. Cells were cultured in Endogrow media for 2 days and then switched to pericyte conditioned medium in RPMI 1640 supplemented with 0.1% FBS to enhance the BBB properties including barrier function and polarity[30, 32].

Immunocytochemistry—The monolayers were washed in PBS, fixed in 4% paraformaldehyde for 10 min, blocked with 10% normal swine serum (Vector Laboratories) for 1 h at room temperature and incubated with different primary antibodies specific for PICALM and LRP1, CHC and LRP1, and PICALM and Rab5, Rab7 or Rab11 overnight at 4°C (see Reagents).

In situ proximity ligation assay (PLA)—The PLA was performed as we previously reported[32].

siRNA and Rab constructs—*si.PICLAM* (catalog # s15799 and s15800), *si.LRP1* (catalog # s8279 and s8280), *si.CHC* (catalog # s475 and s477), *si.RAB11a* (catalog # s16702 and s16703), *si.RAB11b* (catalog # s17647 and s17648) were purchased from Invitrogen. Two siRNAs against distinct sites were used to mitigate against off-target effects. Rab constructs were purchased from Addgene or generated as described in the Reagents section. BEC were transfected using Neon transfection system (Invitrogen) following the manufacturer's instruction.

Rab GTPase activity—Rab5 and Rab11 GTPase activity was determined using Rab5 activation assay kit (NewEast Biosciences, Catalog # 83701) and Rab11 activation assay kit (NewEast Biosciences, Catalog # 83201), respectively.

Adenoviral-mediated transfer—BEC were transduced with adenoviral vectors carrying *PICALM* and *LRP1* minigene[32] 24 h after plating. Cultures were then switched to pericyte conditioned medium within 24 h.

Aβ internalization and transendothelial transport—These experiments were carried out at 37°C. Human unlabeled Aβ40 was added to the basolateral (lower) chamber at a final concentration of 1 nM. The amount of Aβ40 internalized by the monolayers was determined by human Aβ40 ELISA[27]. Aβ uptake by BEC was expressed in pmol/mg protein as we previously described[23]. For transendothelial transport (transcytosis) studies, Aβ40 was added to the basolateral (lower) chamber at a final concentration of 1 nM simultaneously with ^{14}C-inulin (MW~ 5,000), a metabolically inert polar tracer that is not taken up by the vascular cells, as we reported[22, 23]. ^{14}C-inulin was used to correct for the non-specific paracellular leakage of transport across the monolayers, as reported[23, 55]. The intactness of Aβ40 (> 95%) following transport across the BEC monolayer was confirmed in several assay buffer samples from the apical and basolateral chambers using high pressure liquid chromatography, as previously reported[23, 56].

Permeability of the endothelial barrier—We used fluorescein isothiocyanate (FITC) labeled dextrans (40 kDa and 2,000 kDa; Invitrogen), as described[30]. The BBB permeability to dextran was expressed as a permeability coefficient in cm/s as we described[30]. Briefly, the volume cleared (ΔVc) of each time point was calculated using equation #1: $\Delta Vc = C_{lower} \times V_{lower}/C_{upper}$, where C_{upper} and C_{lower} are FITC-labeled dextran concentrations in upper and lower chambers, respectively, and V_{lower} is the volume in lower chamber. The volume cleared (ΔVc) was plotted against time, and the permeability surface area (PS) product was obtained from the slope by linear regression. The permeability coefficient (P) was then

calculated by equation# 2: P = PS/s, where s is the surface area of the filter (1.12 cm^2). Finally, the permeability coefficient of cells (P_{cell}) was obtained by correcting the overall permeability coefficient ($P_{cell+filter}$) for that of the cell-free filter (P_{filter}) using equation #3: $1/P_{cell} = 1/P_{cell+filter} - 1/P_{filter}$. P_{filter} was determined on a separate series of experiments using the cell-free filter inserts only.

iPSC culture

The iPSCs were generated from lymphoblasts from Coriell (Catalog ID: ND10689) using the episomal plasmids, encoding 6 factors *TP53* shRNA, *POU5F1*, *SOX2*, *KLF4*, *MYCL*, and *LIN28A*[46]. These cell lines were maintained on Geltrex (Life Technologies) or Matrigel (BD Bioscience) in mTeSR1 medium (STEMCELL Technologies) supplemented with penicillin/streptomycin.

Construct plasmids for gRNA expression

We used the gRNA Empty Vector from George Church's laboratory that was obtained from Addgene and inserted 20-bp sequence that hybridizes to the DNA target site as described[47]. Briefly, gRNA target sites were selected by the CRISPR design tool developed by Zhang (http://crispr.mit.edu/). Linearize the gRNA cloning vector using AflII and incorporate the DNA fragments into it using Gibson assembly. The following forward (F) and reverse (R) oligos were used for inserts: rs3851179 F: 5′-TTTCTTGGCTTTATATATCTTGTGGAAAGGACGAAACACCGTGAGGTTTACTACTGCAAG-3′ and R: 5′-GACTAGCCTTATTTTAACTTGCTATTTCTAGCTCTAAAACCTTGCAGTAGTAAACCTCAC-3′.

Electroporation

Plasmids were electropoated using Nucleofector™ Kits for Human Dermal Fibroblast (Lonza) according to the manufacturer's protocol. Briefly, after washing with PBS, iPSCs were treated with Accutase (Life Technologies) to dissociate single cells. These cells were suspended with Nucleofector solution and Supplement (Lonza) and mixed with gRNA expression vector, Cas9 coding pSpCas9(BB)-2A-Puro (Addgene) and double-strand plasmid DNA for donor. The donor plasmid was constructed by cloning the flanking regions of rs3851179 amplified by primers as follows; F: 5′- ACCCATCACCCTTCTGTTTG-3′ and R: 5′-TTTTCCAGCAAGTTGGGTTC-3′. Puromycin selections were started at 24 hours after electroporation and continued 3 to 4 days at the concentration of 0.75 μg/mL. After withdrawal of puromycin, cells were cultured in mTeSR until suitably sized colonies appeared. Colonies were picked up and genomic DNAs were extracted using QuickExtract™ DNA Extraction Solution 1.0 (epicentre) according to manufacturer's protocol. Target site was amplified by PCR using primers as follows; F: 5′-CCCGCTTCATAGGGTTATTG-3′ and R: 5′- AACTCACCCCAGTCTCTTGC-3′. We confirmed suspected mutant clones by direct sequencing of the PCR products. We used Sanger sequencing of iPSCs at *rs3851179* to verify independent isogenic lines homozygous for either the G or A variant.

Endothelial differentiation

To generate endothelial cells, we differentiated mutated and original iPSC clones as embryoid bodies (EBs) as described[48]. Two weeks after differentiation, the cells were FACS sorted for endothelial markers CD31 and VE-Cadherin; the isolated double positive cells were characterized with monolayer and tight junction formation, did not express pericyte (PDGFRβ), neuronal (β3-tubulin) or astrocyte (GFAP) markers, and had TEER of ~230 ohms/cm^2 cultured with addition of pericyte-derived conditioned media.

Statistical analysis

Sample sizes were calculated using nQUERY assuming a two-sided alpha-level of 0.05, 80% power, and homogeneous variances for the 2 samples to be compared, with the means and common standard deviation for different parameters predicted from published data and our previous studies. Shapiro-Wilk test was used to test normality of the data, F test was conducted to ensure that the data meets the assumptions of the tests and the variance was similar between the groups that are statistically compared. Data were analyzed by Student's t-test for comparison between two groups; or by multifactorial analysis of variance (ANOVA) followed by Tukey's post hoc tests for multiple comparisons; or paired Wilcoxon's signed rank test for paired non-parametric comparison. Statistical significance for correlation analyses was performed by Pearson and Spearman rank correlation analysis tests. A p value less than 0.05 was considered statistically significant.

Supplementary Material

Refer to Web version on PubMed Central for supplementary material.

Acknowledgments

We would like to thank the National Institutes of Health for grants R37NS34467 (B.V.Z.), R37AG23084 (B.V.Z.), R01AG039452 (B.V.Z.), R01AG035355 (G.B.), R01AG027924 (G.B.), R00NS07743 (J.K.I.), and Cure for Alzheimer Fund (B.V.Z.), American Cancer Society RSG–13–379–01–LIB (T.M.), Rainwater Charitable Foundation (J.K.I.), Donald E. and Delia B. Baxter Foundation (J.K.I.), and Daiichi Sankyo Foundation of Life Science (T.S.). This study used sample ND10689 from the NINDS Cell Line Repository (https://catalog.coriell.org/1/ninds), as well as clinical data.

References

1. Dreyling MH, et al. The t(10;11)(p13;q14) in the U937 cell line results in the fusion of the AF10 gene and CALM, encoding a new member of the AP-3 clathrin assembly protein family. Proc. Natl. Acad. Sci. U.S.A. 1996; 93:4804–4809. [PubMed: 8643484]
2. Tebar F, Bohlander SK, Sorkin A. Clathrin assembly lymphoid myeloid leukemia (CALM) protein: localization in endocytic–coated pits, interactions with clathrin, and the impact of overexpression on clathrin–mediated traffic. Mol. Biol. Cell. 1999; 10:2687–2702. [PubMed: 10436022]
3. Ford MG, et al. Simultaneous binding of PtdIns(4,5)P2 and clathrin by AP180 in the nucleation of clathrin lattices on membranes. Science. 2001; 291:1051–1055. [PubMed: 11161218]
4. Marsh M, McMahon HT. The structural era of endocytosis. Science. 1999; 285:215–220. [PubMed: 10398591]
5. Sorkin A, von Zastrow M. Endocytosis and signalling: intertwining molecular networks. Nat. Rev. Mol. Cell Biol. 2009; 10:609–622. [PubMed: 19696798]
6. Treusch S, et al. Functional links between Aβ toxicity, endocytic trafficking, and Alzheimer's disease risk factors in yeast. Science. 2011; 334:1241–1245. [PubMed: 22033521]

7. Miller SE, et al. The molecular basis for the endocytosis of small R–SNAREs by the clathrin adaptor CALM. Cell. 2011; 147:1118–1131. [PubMed: 22118466]
8. Vecchi M, et al. Nucleocytoplasmic shuttling of endocytic proteins. J. Cell Biol. 2001; 153:1511–1517. [PubMed: 11425879]
9. Harold D, et al. Genome–wide association study identifies variants at CLU and PICALM associated with Alzheimer's disease. Nat. Genet. 2009; 41:1088–1093. [PubMed: 19734902]
10. Lambert JC, et al. Genome–wide association study identifies variants at CLU and CR1 associated with Alzheimer's disease. Nat. Genet. 2009; 41:1094–1099. [PubMed: 19734903]
11. Tanzi RE. The genetics of Alzheimer disease. Cold Spring Harbor Perspect. Med. 2012; 2
12. Lambert JC, et al. Meta–analysis of 74,046 individuals identifies 11 new susceptibility loci for Alzheimer's disease. Nat. Genet. 2013; 45:1452–1458. [PubMed: 24162737]
13. Carrasquillo MM, et al. Late–onset Alzheimer disease genetic variants in posterior cortical atrophy and posterior AD. Neurology. 2014; 82:1455–1462. [PubMed: 24670887]
14. Zlokovic BV. Neurovascular pathways to neurodegeneration in Alzheimer's disease and other disorders. Nat. Rev. Neurosci. 2011; 12:723–738. [PubMed: 22048062]
15. Hardy J, Selkoe DJ. The amyloid hypothesis of Alzheimer's disease: progress and problems on the road to therapeutics. Science. 2002; 297:353–356. [PubMed: 12130773]
16. Querfurth HW, LaFerla FM. Alzheimer's disease. N. Engl. J. Med. 2010; 362:329–344. [PubMed: 20107219]
17. Tian Y, Chang JC, Fan EY, Flajolet M, Greengard P. Adaptor complex AP2/PICALM, through interaction with LC3, targets Alzheimer's APP–CTF for terminal degradation via autophagy. Proc. Natl. Acad. Sci. U.S.A. 2013; 110:17071–17076. [PubMed: 24067654]
18. Xiao Q, et al. Role of phosphatidylinositol clathrin assembly lymphoid–myeloid leukemia (PICALM) in intracellular amyloid precursor protein (APP) processing and amyloid plaque pathogenesis. J. Biol. Chem. 2012; 287:21279–21289. [PubMed: 22539346]
19. Kanatsu K, et al. Decreased CALM expression reduces Aβ42 to total Aβ ratio through clathrin–mediated endocytosis of γ–secretase. Nat Commun. 2014; 5:3386. [PubMed: 24577224]
20. Baig S, et al. Distribution and expression of picalm in Alzheimer disease. J. Neuropathol. Exp. Neurol. 2010; 69:1071–1077. [PubMed: 20838239]
21. Parikh I, Fardo DW, Estus S. Genetics of PICALM expression and Alzheimer's disease. PloS One. 2014; 9:e91242. [PubMed: 24618820]
22. Shibata M, et al. Clearance of Alzheimer's amyloid–ss(1–40) peptide from brain by LDL receptor–related protein–1 at the blood–brain barrier. J. Clin. Invest. 2000; 106:1489–1499. [PubMed: 11120756]
23. Deane R, et al. LRP/amyloid beta–peptide interaction mediates differential brain efflux of Abeta isoforms. Neuron. 2004; 43:333–344. [PubMed: 15294142]
24. Wu Z, et al. Role of the MEOX2 homeobox gene in neurovascular dysfunction in Alzheimer disease. Nat. Med. 2005; 11:959–965. [PubMed: 16116430]
25. Bell RD, et al. SRF and myocardin regulate LRP–mediated amyloid–beta clearance in brain vascular cells. Nat. Cell Biol. 2009; 11:143–153. [PubMed: 19098903]
26. Kanekiyo T, Liu CC, Shinohara M, Li J, Bu G. LRP1 in brain vascular smooth muscle cells mediates local clearance of Alzheimer's amyloid–β. J. Neurosci. Off. J. Soc. Neurosci. 2012; 32:16458–16465.
27. Sagare AP, et al. Pericyte loss influences Alzheimer–like neurodegeneration in mice. Nat. Commun. 2013; 4:2932. [PubMed: 24336108]
28. Ando K, et al. Clathrin adaptor CALM/PICALM is associated with neurofibrillary tangles and is cleaved in Alzheimer's brains. Acta Neuropathol. (Berl.). 2013; 125:861–878. [PubMed: 23589030]
29. Hsiao K, et al. Correlative memory deficits, Abeta elevation, and amyloid plaques in transgenic mice. Science. 1996; 274:99–102. [PubMed: 8810256]
30. Zhu D, et al. Protein S controls hypoxic/ischemic blood–brain barrier disruption through the TAM receptor Tyro3 and sphingosine 1–phosphate receptor. Blood. 2010; 115:4963–4972. [PubMed: 20348395]

31. Li Y, Lu W, Marzolo MP, Bu G. Differential functions of members of the low density lipoprotein receptor family suggested by their distinct endocytosis rates. J. Biol. Chem. 2001; 276:18000–18006. [PubMed: 11279214]
32. Bell RD, et al. Apolipoprotein E controls cerebrovascular integrity via cyclophilin A. Nature. 2012; 485:512–516. [PubMed: 22622580]
33. Armulik A, et al. Pericytes regulate the blood–brain barrier. Nature. 2010; 468:557–561. [PubMed: 20944627]
34. Bell RD, et al. Pericytes control key neurovascular functions and neuronal phenotype in the adult brain and during brain aging. Neuron. 2010; 68:409–427. [PubMed: 21040844]
35. Daneman R, Zhou L, Kebede AA, Barres BA. Pericytes are required for blood–brain barrier integrity during embryogenesis. Nature. 2010; 468:562–566. [PubMed: 20944625]
36. Winkler EA, Bell RD, Zlokovic BV. Pericyte–specific expression of PDGF beta receptor in mouse models with normal and deficient PDGF beta receptor signaling. Mol. Neurodegener. 2010; 5:32. [PubMed: 20738866]
37. Kanekiyo T, et al. Neuronal clearance of amyloid–β by endocytic receptor LRP1. J. Neurosci. Off. J. Soc. Neurosci. 2013; 33:19276–19283.
38. Stenmark H. Rab GTPases as coordinators of vesicle traffic. Nat. Rev. Mol. Cell Biol. 2009; 10:513–525. [PubMed: 19603039]
39. Li J, et al. Differential regulation of amyloid–β endocytic trafficking and lysosomal degradation by apolipoprotein E isoforms. J. Biol. Chem. 2012; 287:44593–44601. [PubMed: 23132858]
40. Xu S, et al. A Rab11a–enriched subapical membrane compartment regulates a cytoskeleton–dependent transcytotic pathway in secretory epithelial cells of the lacrimal gland. J. Cell Sci. 2011; 124:3503–3514. [PubMed: 21984810]
41. Lapierre LA, et al. Phosphorylation of Rab11–FIP2 regulates polarity in MDCK cells. Mol. Biol. Cell. 2012; 23:2302–2318. [PubMed: 22553350]
42. Yui N, et al. Basolateral targeting and microtubule–dependent transcytosis of the aquaporin-2 water channel. Am. J. Physiol. Cell Physiol. 2013; 304:C38–C48. [PubMed: 23015545]
43. Takahashi S, et al. Rab11 regulates exocytosis of recycling vesicles at the plasma membrane. J. Cell Sci. 2012; 125:4049–4057. [PubMed: 22685325]
44. Zeigerer A, et al. Rab5 is necessary for the biogenesis of the endolysosomal system in vivo. Nature. 2012; 485:465–470. [PubMed: 22622570]
45. Raj T, et al. Alzheimer disease susceptibility loci: evidence for a protein network under natural selection. Am. J. Hum. Genet. 2012; 90:720–726. [PubMed: 22482808]
46. Okita K, et al. A more efficient method to generate integration–free human iPS cells. Nat. Methods. 2011; 8:409–412. [PubMed: 21460823]
47. Mali P, et al. RNA–guided human genome engineering via Cas9. Science. 2013; 339:823–826. [PubMed: 23287722]
48. Adams WJ, et al. Functional vascular endothelium derived from human induced pluripotent stem cells. Stem Cell Rep. 2013; 1:105–113.
49. Bushlin I, et al. Clathrin assembly protein AP180 and CALM differentially control axogenesis and dendrite outgrowth in embryonic hippocampal neurons. J. Neurosci. Off. J. Soc. Neurosci. 2008; 28:10257–10271.
50. Harel A, Mattson MP, Yao PJ. CALM, a clathrin assembly protein, influences cell surface GluR2 abundance. Neuromolecular Med. 2011; 13:88–90. [PubMed: 21221849]

Supplementary References

51. Zlokovic BV, Mackic JB, Wang L, McComb JG, McDonough A. Differential expression of Na,K-ATPase alpha and beta subunit isoforms at the blood-brain barrier and the choroid plexus. J. Biol. Chem. 1993; 268:8019–8025. [PubMed: 8385133]
52. Wu Z, Hofman FM, Zlokovic BV. A simple method for isolation and characterization of mouse brain microvascular endothelial cells. J. Neurosci. Methods. 2003; 130:53–63. [PubMed: 14583404]

53. Cirrito JR, et al. P-glycoprotein deficiency at the blood-brain barrier increases amyloid-beta deposition in an Alzheimer disease mouse model. J. Clin. Invest. 2005; 115:3285–3290. [PubMed: 16239972]

54. Grimm D, et al. In vitro and in vivo gene therapy vector evolution via multispecies interbreeding and retargeting of adeno-associated viruses. J. Virol. 2008; 82:5887–5911. [PubMed: 18400866]

55. Mackic JB, et al. Human blood-brain barrier receptors for Alzheimer's amyloid-beta 1–40. Asymmetrical binding, endocytosis, and transcytosis at the apical side of brain microvascular endothelial cell monolayer. J. Clin. Invest. 1998; 102:734–743. [PubMed: 9710442]

56. Deane R, et al. RAGE mediates amyloid-beta peptide transport across the blood-brain barrier and accumulation in brain. Nat. Med. 2003; 9:907–913. [PubMed: 12808450]

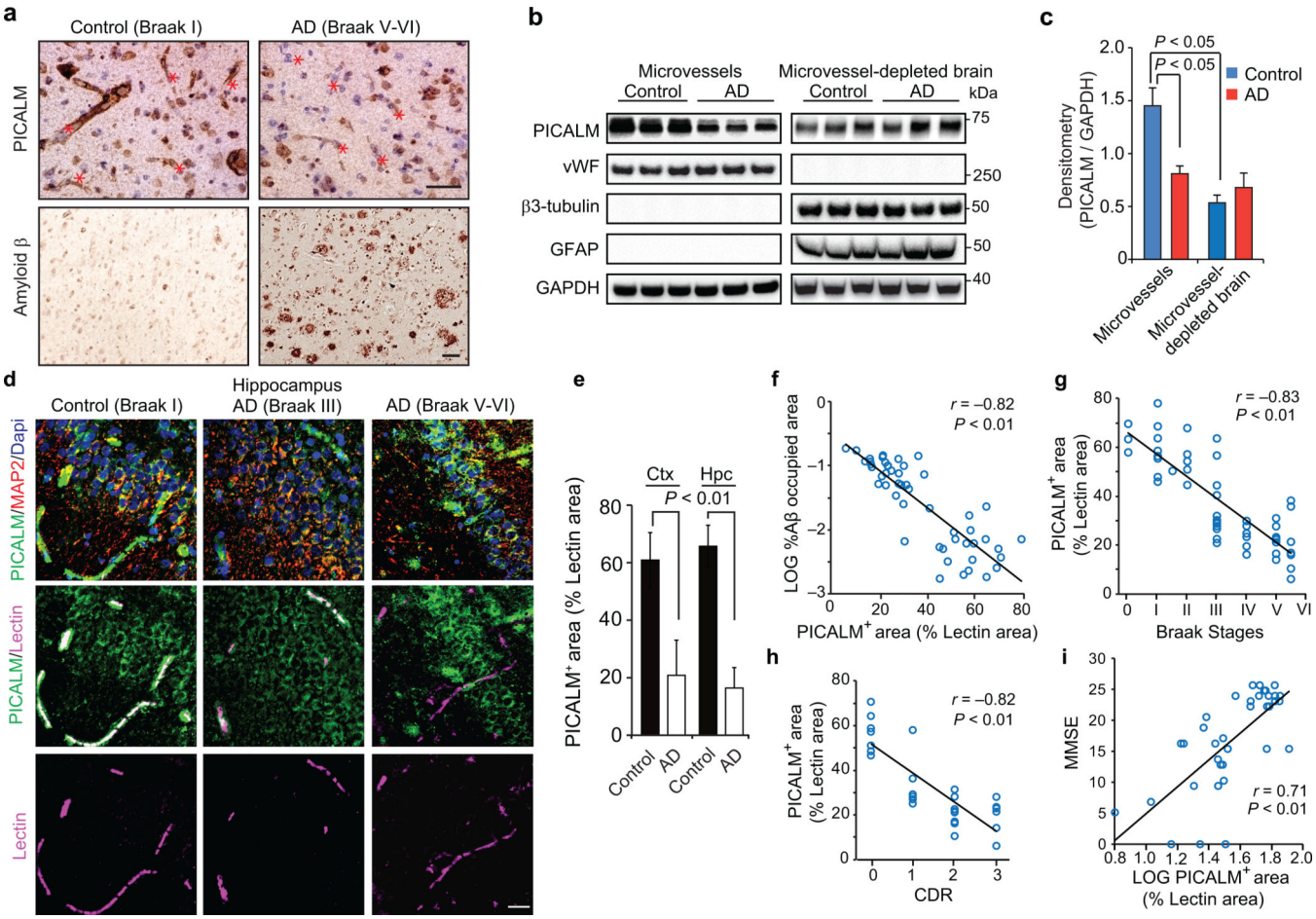

Figure 1. PICALM reductions in brain capillary endothelium in Alzheimer's disease

a, PICALM and Aβ immunostaining in the prefrontal cortex of an age–matched control (Braak I, left) and AD case (Braak V–VI, right). Bar=20 μm. **b**, Immunoblotting for PICALM, von Willebrand Factor (vWF), β3–tubulin, glial fibrillar acidic protein (GFAP), and GAPDH (loading control) in isolated microvessels and microvessel–depleted brains from controls (Braak 0–I) and AD cases (Braak V–VI). **c**, Relative abundance of PICALM in microvessels and microvessel–depleted brains from control and AD cases determined by densitometry analysis relative to GAPDH. Mean ± s.e.m., n=6/group; $p<0.05$ by ANOVA followed by Tukey's posthoc tests. **d**, PICALM (green), lectin–positive endothelial capillary profiles (magenta) and microtubule–associated protein 2 (MAP2)–positive neurons (red) in the hippocampus (CA1) of an age–matched control (Braak I) and AD cases (Braak III and V–VI). Bar=20 μm. **e**, Quantification of PICALM–positive area (percentage) occupying lectin–positive endothelial capillary profiles in the prefrontal cortex and the CA1 hippocampal subfield. Mean ± s.d., n=9 controls (Braak 0–I) and 7 AD cases (Braak V–VI); $p<0.01$ by Student's t–test. **f–i**, Correlations between PICALM–positive area occupying lectin–positive endothelial capillary profiles (percentage) in the prefrontal cortex and Aβ load (**f**), Braak stages (**g**), Clinical Dementia Rating (CDR) (**h**), and Mini–Mental State Examination (MMSE) (**i**). Each point in **f–i** is an individual value from 50 (**f–g**), 28 (**h**) and

37 (**i**) controls and AD cases. CDR and MMSE were not available for all cases. Significance by Pearson and Spearman rank correlation analysis.

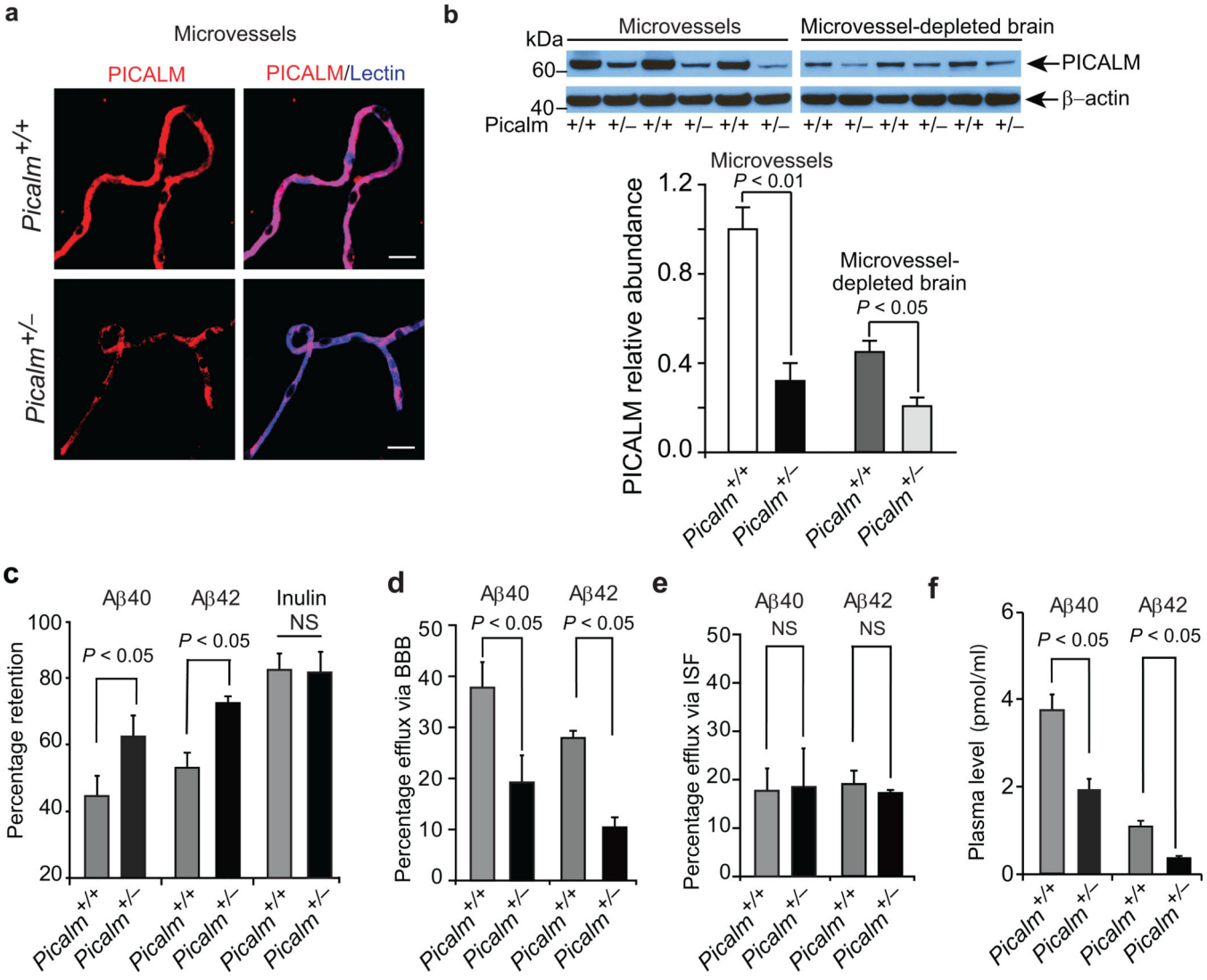

Figure 2. Diminished Aβ clearance in *Picalm*$^{+/-}$ mice

a, Immunostaining for PICALM (red) and endothelial–specific lectin (blue) in brain microvessels from *Picalm*$^{+/+}$ and *Picalm*$^{+/-}$ mice. **b**, Relative abundance of PICALM protein compared to β–actin studied by immunoblotting and densitometry analysis in brain microvessels and microvessel–depleted brain homogenates in *Picalm*$^{+/+}$ and *Picalm*$^{+/-}$ mice. P<0.05 by Student's t–test; NS, non–significant. Means ± s.e.m. from 3–4 mice per group. **c–f**, Brain retention of Aβ40 (left), Aβ42 (middle) and ^{14}C–inulin (right) (**c**), Aβ40 and Aβ42 clearance across the BBB (**d**) and by interstitial fluid (ISF) bulk flow (**e**) and plasma levels of Aβ40 or Aβ42 (**f**) after 30 min of intracerebral administration of human synthetic Aβ40, Aβ42 and ^{14}C–inulin into the caudate nucleus of 3 month old *Picalm*$^{+/+}$ and *Picalm*$^{+/-}$ mice. Aβ in brain and plasma was determined using human–specific Aβ40 or Aβ42 ELISA. Means ± s.e.m., n=6 mice per group. Statistical significance by Student's t–test. NS, non–significant. p<0.05 by Student's t–test. NS, non–significant.

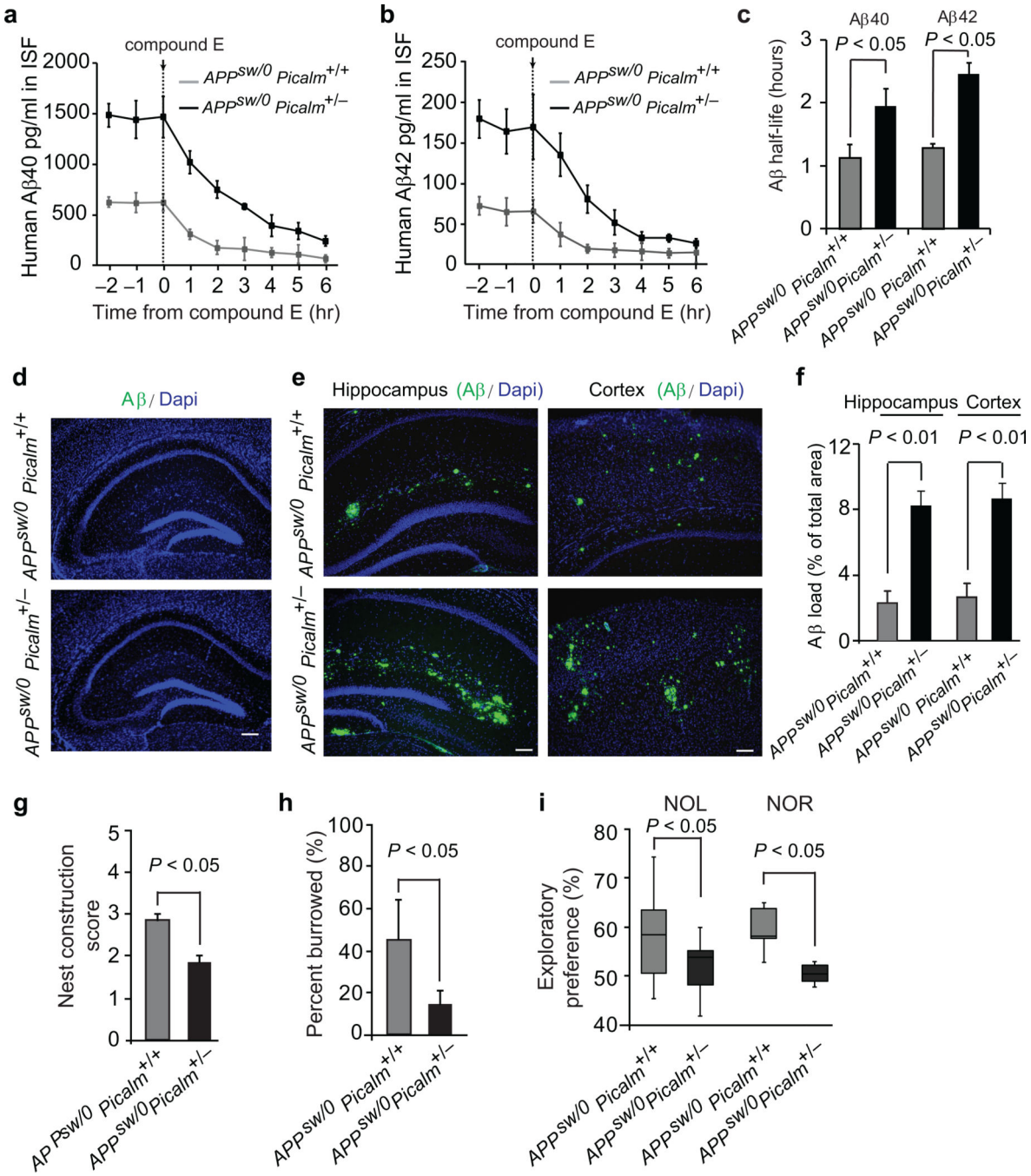

Figure 3. Diminished Aβ clearance and accelerated pathology in *APP*$^{sw/0}$ *Picalm*$^{+/-}$ mice

a–b, ISF $A\beta_{40}$ and $A\beta_{42}$ levels monitored by *in vivo* hippocampal microdialysis of 3 month old *APP*$^{sw/0}$; *Picalm*$^{+/-}$ and *APP*$^{sw/0}$; *Picalm*$^{+/+}$ mice. Baseline Aβ levels were monitored for 3 hours. **c**, The elimination half–life of ISF Aβ40 and Aβ42 determined after administration of compound E (γ–secretase inhibitor) 20 mg/kg intraperitoneally. **d**, Representative cortex and hippocampus sections stained with human Aβ specific antibodies in 3 month old *APP*$^{sw/0}$; *Picalm*$^{+/+}$ and *APP*$^{sw/0}$; *Picalm*$^{+/-}$ mice, showing no Aβ deposition. Bar: 100 μm. **e–f**, Representative hippocampus and cortex sections stained with

human Aβ specific antibodies in 9 month old *APP*$^{sw/0}$; *Picalm*$^{+/+}$ and *APP*$^{sw/0}$; *Picalm*$^{+/-}$ mice, showing accelerated Aβ deposition (**e**) and increased Aβ load (**f**). In **c** and **f**, means ± s.e.m., n=5–6 mice per group. **g–i**, Behavioral changes in 9 month old *APP*$^{sw/0}$; *Picalm*$^{+/+}$ and *APP*$^{sw/0}$; *Picalm*$^{+/-}$ mice studied by nest construction (**g**), burrowing (**h**), novel object location (NOL) and novel object recognition (NOR) (**i**). Means ± s.e.m. n=12–14 mice per group. In **g–i**, statistical significance by Student's t–test. In **i**, boxplots represent the median (dark horizontal line), with the box representing the 25th and 75th percentiles, the whiskers the 5th and 95th percentile.

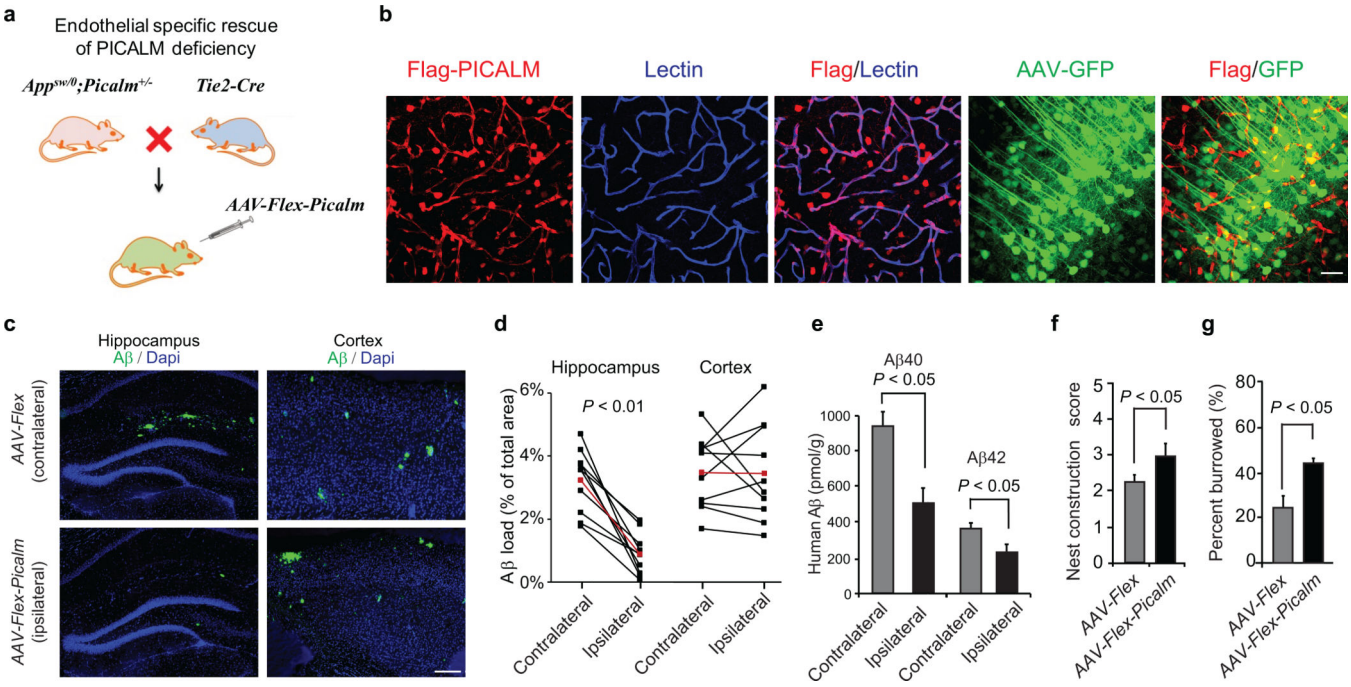

Figure 4. Endothelial specific rescue of PICALM deficiency in the hippocampus of *APP$^{sw/0}$ Picalm$^{+/-}$* mice

a, The scheme of endothelial specific rescue of PICALM in *APP$^{sw/0}$*; *Picalm$^{+/-}$*; *Tie2–Cre* mice using adeno–associated virus (*AAV*) carrying a Cre recombinase dependent expression cassette of *Flag–Picalm* transgene (see Methods for details). **b**, Expression of Flag–PICALM in endothelium of 5 month old *APP$^{sw/0}$*; *Picalm$^{+/-}$*; *Tie2–Cre* mouse after *AAV–Flex–Picalm* administration in the hippocampus. Lectin, endothelial specific marker. Co–injection of *AAV–Synapsin–GFP* shows insignificant expression of Flag–PICALM in neurons (< 3%). **c–e**, Endothelial–specific expression of PICALM in the ipsilateral hippocampus of *APP$^{sw/0}$*; *Picalm$^{+/-}$*; *Tie2–Cre* mice injected with *AAV–Flex–Picalm* (see **b**) reduces Aβ deposition (**c–d**) and Aβ40 and Aβ42 accumulation (**e**) at 6 months of age compared to the contralateral hippocampus injected with *AAV–Flex* control. Cortex that was not injected with *AAV–Flex–Picalm* shows no changes in Aβ load (**c, d**). Red lines in **d** indicate average values. P<0.01 by paired Wilcoxon Signed Rank Test. **f–g**, Bilateral hippocampal administration of *AAV–Flex–Picalm* compared to *AAV–Flex* (control) improves behavior in 6 month old *APP$^{sw/0}$*; *Picalm$^{+/-}$*; *Tie2–Cre* mice. Means ± s.e.m., n=10 mice per group. p<0.05 by Student's t–test.

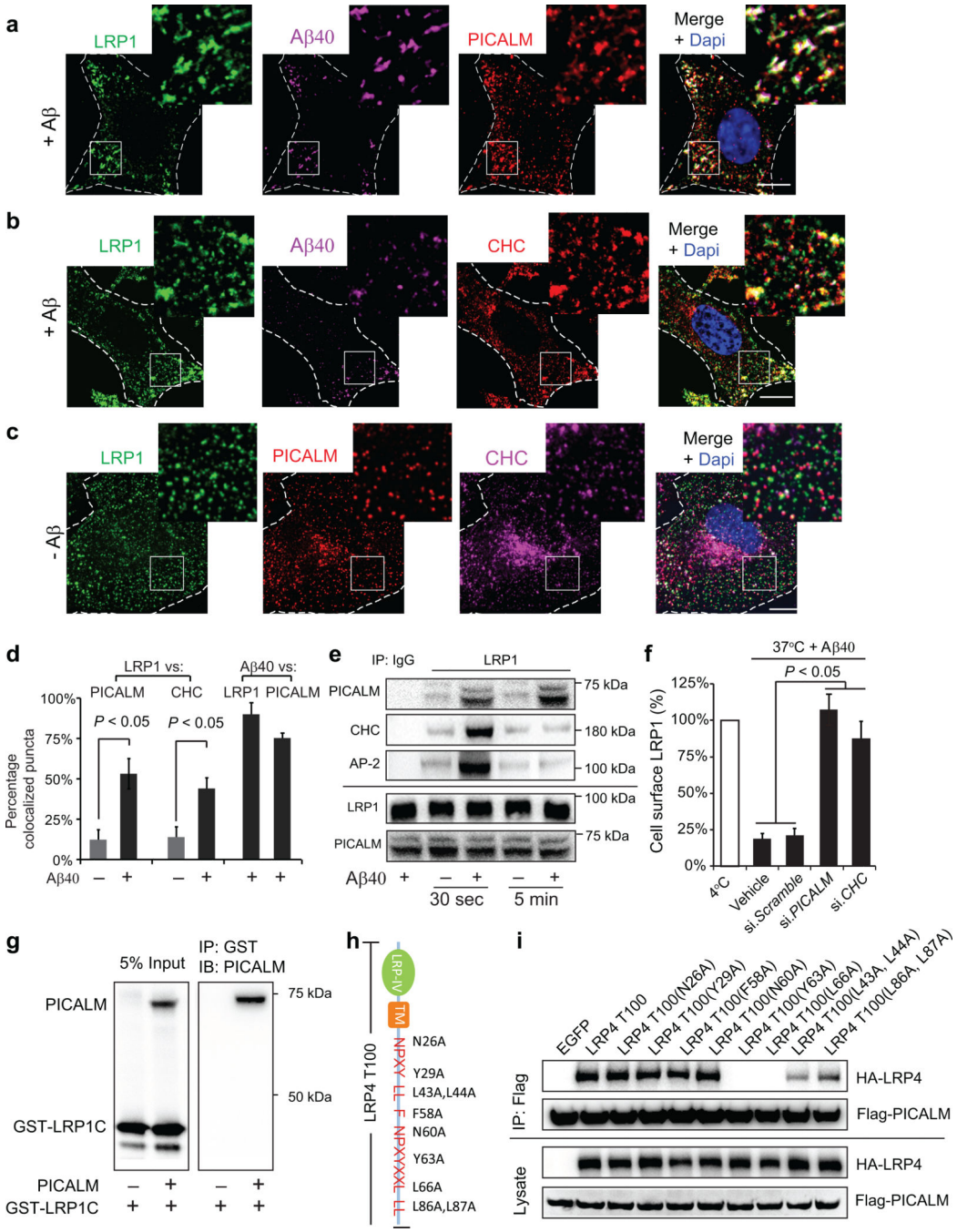

Figure 5. PICALM/clathrin–dependent endocytosis of Aβ–LRP1 complex by brain endothelial cells

a–b, Colocalization of LRP1–Aβ40 complex with PICALM (**a**) and clathrin heavy chain (CHC) (**b**) in human brain endothelial cells (BEC) within 30 s of FAM–Aβ40 (250 nM) treatment. **c**, Immunostaining for LRP1, PICALM and CHC without Aβ (– Aβ). Dapi, nuclear staining (blue). Insets: higher magnification. Bar=10 μm. **d**, Quantification of LRP1 puncta colocalized with PICALM in **a, c** and with CHC in **b, c**, and FAM–Aβ40 puncta colocalized with LRP1 and PICALM in **a, b**. Means ± s.d. from 3 primary isolates in

triplicate. $p<0.05$ by Student's t–test. **e**, Coimmunoprecipitation of PICALM, CHC and clathrin adaptor protein α–adaptin (AP–2) by LRP1–specific antibody (IP: LRP1) in BEC 30 s or 5 min after stimulation with Aβ40 (1 nM); IgG, non–immune IgG. **f**, LRP1 internalization in control BEC (vehicle) and after transfection with si.*Scramble* RNA and/or si.RNAs targeting *PICALM* or *CHC.* Aβ40 (1 nM) was applied for 15 min at 4°C followed by 1 min at 37°C to initiate LRP1 internalization. Values at 4°C were taken as 100%. Means ± s.d. from 3 primary isolates in triplicate. $p<0.05$ by ANOVA followed by Tukey's posthoc tests. **g**, *In vitro* binding of human recombinant PICALM to GST–tagged LRP1 C–terminus fusion protein (GST–LRP1C). **h**, C–terminal mutants of the human LRP1 minigene (LRP4T100). **i**, Coimmunoprecipitation of HA–tagged C–terminal LRP1 mutants (LRP4T100) by anti–Flag antibody (IP: Flag) in HEK293T cells after transfection with Flag–PICALM and HA–LRP4T100 mutants. HA–LRP4 and Flag–PICALM were used as loading controls.

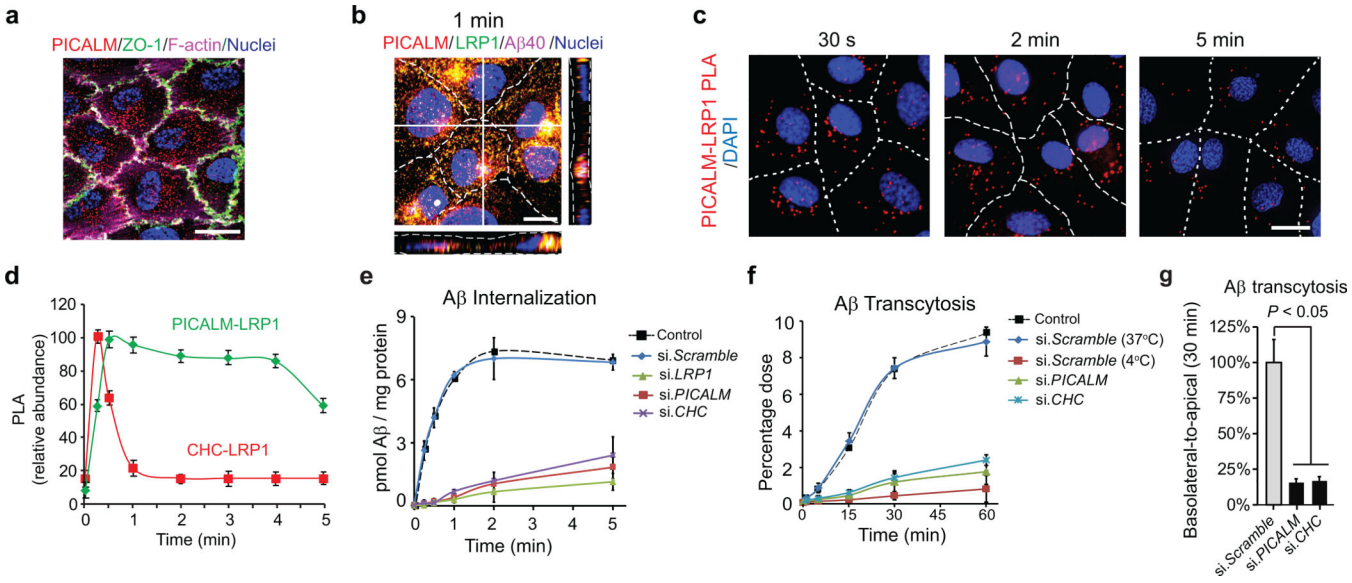

Figure 6. PICALM associates with LRP1 during Aβ transcytosis across endothelial monolayer

a, PICALM (red), ZO–1 (green) and F–actin (magenta) in a monolayer. **b**, Colocalization of PICALM (red) with LRP1 (green) and FAM–Aβ40 (magenta) 1 min after LRP1–Aβ internalization at the basolateral membrane. **c–d**, Proximity ligation assay (PLA) depicting PICALM–LRP1 association (**c**, bar=10 μm) and kinetics of association between PICALM and LRP1 and clathrin and LRP1 in endothelium after Aβ40 (1 nM) addition to the basolateral membrane studied by PLA (**d**). **e**, Internalization of Aβ40 (1 nM) at the basolateral membrane of the monolayer transfected with si.*LRP1*, si.*PICALM* and si.*CHC* compared si.*Scramble* or untransfected control. **f–g**, Basolateral–to–apical transcytosis of Aβ40 (1 nM) across endothelial monolayer transfected with si.*PICALM* and si.*CHC* compared to si.*Scramble* (100%) over 60 min (**f**) and quantification of unidirectional trans–endothelial Aβ40 transport within 30 min (**g**). Mean ± s.e.m. from 3 primary isolates in triplicates. $p<0.05$ by ANOVA followed by Tukey's posthoc test.

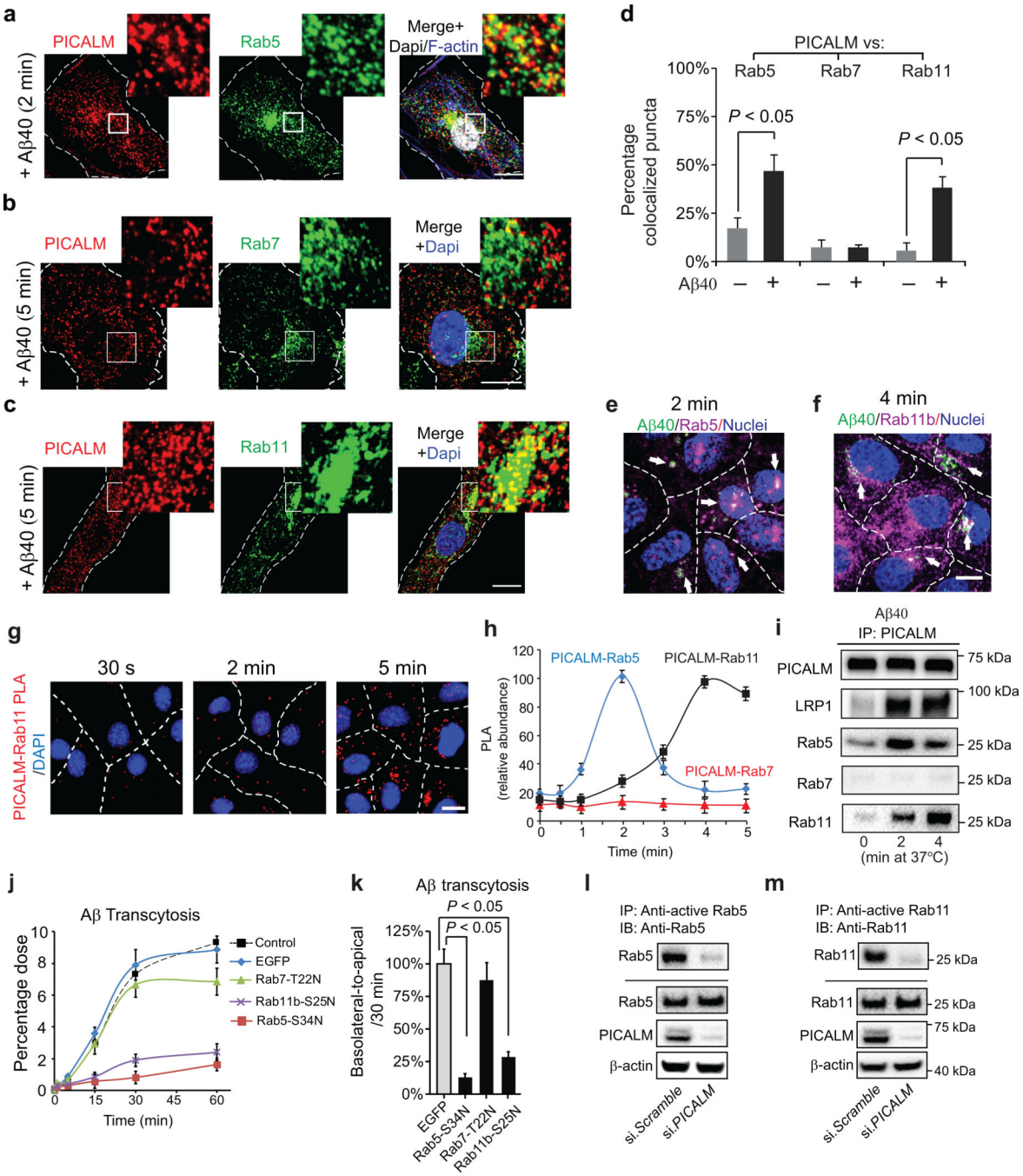

Figure 7. PICALM interacts with Rab5 and Rab11 during Aβ transcytosis across endothelial monolayer

a, Colocalization between PICALM (red) and Rab5 (green) in primary human brain endothelial cells (BEC) cultured with FAM–Aβ40 (250 nM) for 2 min. **b**, Lack of association between PICALM (red) and Rab7 (green) in BEC cultured with FAM–Aβ40 for 5 min. **c**, Colocalization between PICALM (red) and Rab11 (green) in BEC cultured with FAM–Aβ40 for 5 min. Dapi, nuclear staining (blue). Insets: high magnification depicting colocalization. Bar=10 μm. **d**, Quantification of colocalization between PICALM and Rab5,

Rab7, or Rab11 puncta in **a–c**. **e–f**, Colocalization of FAM–Aβ40 (green) with Rab5 (magenta, *upper*) or RAB11b (magenta, *bottom*) 2 and 4 min after Aβ internalization at the basolateral side of endothelial monolayer, respectively. Arrows denote co–localized white puncta. **g–h**, PLA of PICALM–Rab11 association (**g**, bar=10 μm) and kinetics of PICALM association with Rab5, Rab7 and Rab11 in endothelium after addition of Aβ40 (1 nM) to the basolateral membrane (**h**). **i**, Coimmunoprecipitation of LRP1, Rab5, Rab7 and Rab11 by PICALM–specific antibody (IP: PICALM) 0, 2 and 4 min after addition of Aβ40 (1 nM) to the basloateral membrane. **j–k**, Basolateral–to–apical transcytosis of Aβ40 (1 nM) across monolayer expressing dominant negative Rab5–S34N, Rab7–T22N or Rab11b–S25N mutants compared to control EGFP (100%) over 60 min (**j**) and quantification of unidirectional Aβ40 transport within 30 min (**k**). Mean ± s.e.m. from 3 primary isolates in triplicates. $p<0.05$ by ANOVA followed by Tukey's posthoc test. **l–m,** Inhibition of Rab5 (**l**) and Rab11 (**m**) GTPase activity by si.*PICALM* compared to si.*Scramble* control.

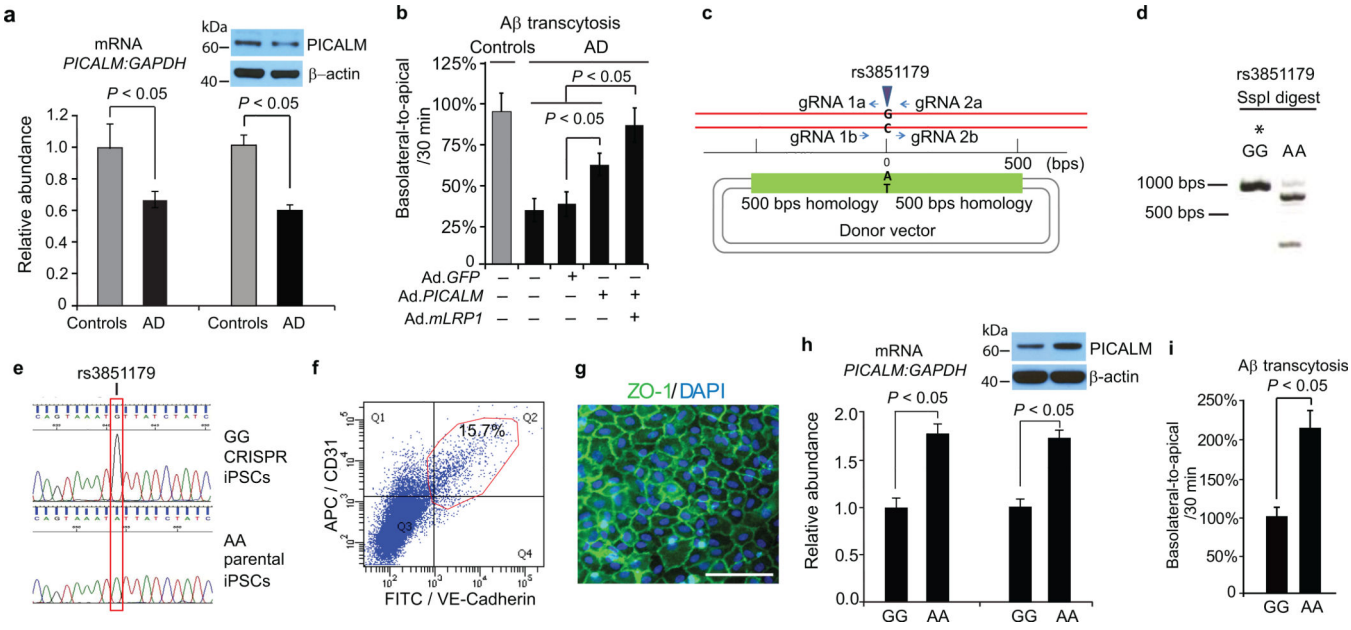

Figure 8. Aβ transcytosis across AD–derived endothelial monolayer and iPSC–derived endothelium carrying the *rs3851179 PICALM* variants

a, qRT–PCR and western blot analysis of PICALM in control and AD endothelial monolayers. **b**, Diminished Aβ40 (1 nM) transcytosis across AD–derived endothelium and reversal by adenoviral–mediated Ad.*PICALM* re–expression. Ad.*mLRP1*, *LRP1* minigene. Mean ± s.e.m., from 8 isolates in triplicate for control and AD monolayers. **c**, Diagram of CRISPR/Cas9–based generation of isogenic iPSC lines homozygous for the protective (A) or non–protective (G) allele of *rs3851179*. gRNA = guide RNA. **d**, SspI restriction digest of PCR products from iPSC genomic DNA at *rs3851179* region. *denotes the CRISPR–Cas9 modified iPSC line. **e**, Sanger sequencing of iPSCs at *rs3851179* confirming independent isogenic lines homozygous for either the G or A variant. **f**, FACS dot plot showing 15.7% of iPSC–derived endothelial cells via embryoid body (EB) formation are positive for endothelial markers CD31 and VE–Cadherin. **g**, iPSC–derived endothelial cells co–cultured with pericyte conditioned media form monolayer *in vitro* with ZO–1 positive tight junctions (green). Bar=100 μm. **h–i**, qRT–PCR and western blot analysis of PICALM (**h**) and Aβ40 (1 nM) transcytosis (**i**) in human iPSC–derived endothelial monolayers carrying the protective *rs3851179* (AA) variant and the non–protective *rs3851179* (GG) variant. In **h–i**, means ± s.e.m., from 6 cultures for each *rs3851179* variant in triplicates.